Cell Chemical Biology

Characterization of Small-Molecule-Induced Changes in Parkinson's-Related Trafficking via the Nedd4 Ubiquitin Signaling Cascade

Graphical Abstract

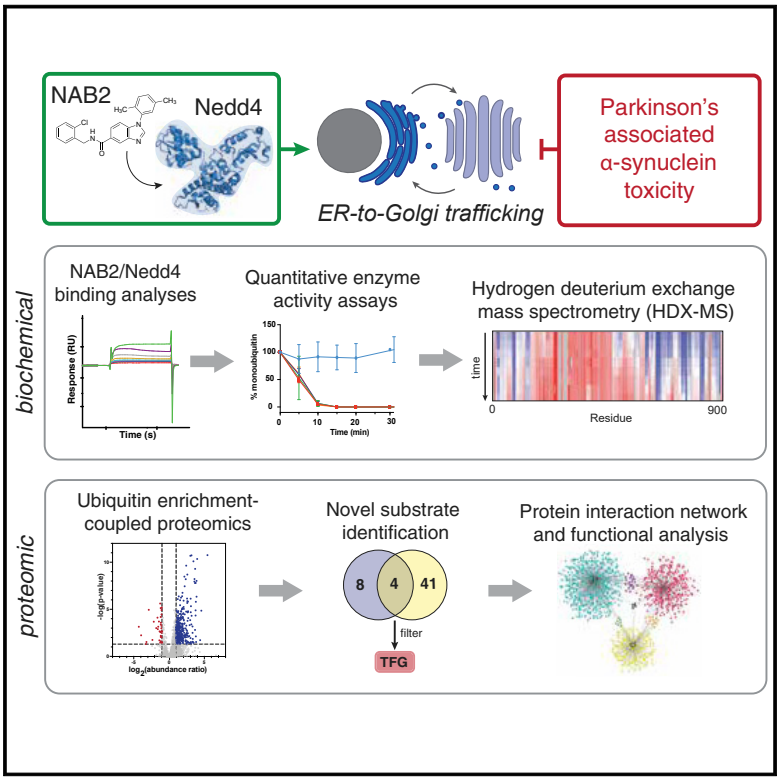

Highlights

- NAB2 binds to Nedd4 with apparent affinity in the nanomolar range
- NAB2 treatment does not induce changes in Nedd4 activity or conformation *in vitro*
- α-Synuclein toxicity drastically changes global protein ubiquitination
- NAB2 treatment of toxic cells reveals novel Nedd4 target and trafficking network

Authors

A. Katherine Hatstat, Hannah D. Ahrendt, Matthew W. Foster, Leland Mayne, M. Arthur Moseley, S. Walter Englander, Dewey G. McCafferty

Correspondence

dewey.mccafferty@duke.edu

In Brief

N-Arylbenzdiimidazole ligand NAB2 was previously shown to rescue Parkinson's-related toxicity in cellular models in a manner dependent upon E3 ubiquitin ligase Nedd4. Here, Hatstat et al. report a biochemical and proteomic characterization of the NAB2 mechanism, advancing our understanding of NAB2 and Nedd4 as anti-parkinsonian lead and target, respectively.

Hatstat et al., 2021, Cell Chemical Biology *28*, 14–25
January 21, 2021
https://doi.org/10.1016/j.chembiol.2020.10.008

CellPress

CellPress

Cell Chemical Biology

Article

Characterization of Small-Molecule-Induced Changes in Parkinson's-Related Trafficking via the Nedd4 Ubiquitin Signaling Cascade

A. Katherine Hatstat,[1] Hannah D. Ahrendt,[1] Matthew W. Foster,[3] Leland Mayne,[4,5] M. Arthur Moseley,[3] S. Walter Englander,[4,5] and Dewey G. McCafferty[1,2,6,*]

[1]Department of Chemistry, Duke University, Durham, NC 27708, USA
[2]Department of Biochemistry, School of Medicine, Duke University, Durham, NC 27710, USA
[3]Proteomics and Metabolomics Core Facility, Duke University Medical Center, Durham, NC 27710, USA
[4]Johnson Research Foundation, Perelman School of Medicine, University of Pennsylvania, Philadelphia, PA 19355, USA
[5]Department of Biochemistry and Biophysics, Perelman School of Medicine, University of Pennsylvania, Philadelphia, PA 19355, USA
[6]Lead Contact
*Correspondence: dewey.mccafferty@duke.edu
https://doi.org/10.1016/j.chembiol.2020.10.008

SUMMARY

The benzdiimidazole NAB2 rescues α-synuclein-associated trafficking defects associated with early onset Parkinson's disease in a Nedd4-dependent manner. Despite identification of E3 ubiquitin ligase Nedd4 as a putative target of NAB2, its molecular mechanism of action has not been elucidated. As such, the effect of NAB2 on Nedd4 activity and specificity was interrogated through biochemical, biophysical, and proteomic analyses. NAB2 was found to bind Nedd4 (K_D^{app} = 42 nM), but this binding is side chain mediated and does not alter its conformation or ubiquitination kinetics *in vitro*. Nedd4 co-localizes with trafficking organelles, and NAB2 exposure did not alter its co-localization. Ubiquitin enrichment coupled proteomics revealed that NAB2 stimulates ubiquitination of trafficking-associated proteins, most likely through modulating the substrate specificity of Nedd4, providing a putative protein network involved in the NAB2 mechanism and revealing trafficking scaffold protein TFG as a Nedd4 substrate.

INTRODUCTION

Parkinson's disease (PD), a neurodegenerative disorder characterized by distinct motor and non-motor symptoms, results from targeted loss of dopaminergic neurons in the midbrain. Neurodegeneration can result from many causes, including cellular toxicity induced by aggregation of toxic proteins. In one type of PD, mutations, duplications, or triplications at the *SNCA* gene locus induce production of toxic proteoforms of α-synuclein (Lashuel et al., 2013; Rocha et al., 2018; Singleton et al., 2003; Tardiff et al., 2013). In its wild-type (WT) form, α-synuclein is a membrane-associated protein involved in trafficking processes. In the presence of PD-associated *SNCA* alterations, α-synuclein forms toxic aggregates that induce generation of reactive oxygen species and disrupt cellular processes, including trafficking and transport (Cooper et al., 2006; Del Mar et al., 2005; Gitler et al., 2008; Outeiro et al., 2003).

There is increased interest in treatments for PD that target disrupted cellular processes associated with neuronal toxicity to support front-line dopamine replacement therapy. Pharmacological alleviation of neurotoxicity could prevent further neurodegeneration and help mitigate some disease-related sequelae, such as reduced sensitivity to levodopa over extended periods of use (Lesser et al., 1979; Marsden and Parkes, 1976; Munchau and Bhatia, 2000; Riley and Lang, 1993). Identifying critical neurotoxicity signaling players has led to the development of cellular models for phenotype-driven screening for identification of targets and potential small-molecule leads to reverse neurotoxicity. Recently, the Lindquist group developed a yeast-based phenotypic model of α-synuclein toxicity and discovered a small-molecule *N*-arylbenzdiimidazole (NAB) that significantly alleviated major phenotypic markers of α-synuclein toxicity (Figure 1A) (Chung et al., 2013; Tardiff et al., 2013). Counter genetic screening revealed that the activity of NAB analogs (NABs) depended upon the yeast protein Rsp5, an E3 ubiquitin ligase. Further validation in mammalian cell models indicated that NAB activity was conserved and dependent upon Nedd4, the mammalian homolog of Rsp5. Finally, structure-activity relationship (SAR) optimization of the NAB scaffold afforded a derivative, NAB2, with improved activity over the lead compound (Figure 1A) (Tardiff et al., 2013). However, since these initial studies, the molecular mechanism of NAB2 and the role of Nedd4 in the alleviation of toxicity have yet to be further elucidated.

The identification of Nedd4 as a potential target in PD-associated toxicity is intriguing for a number of reasons. Nedd4 has previously been implicated in cellular responses to PD-associated toxicity as it was shown to ubiquitinate α-synuclein, resulting in ubiquitination-induced degradation of the protein (Tofaris et al.,

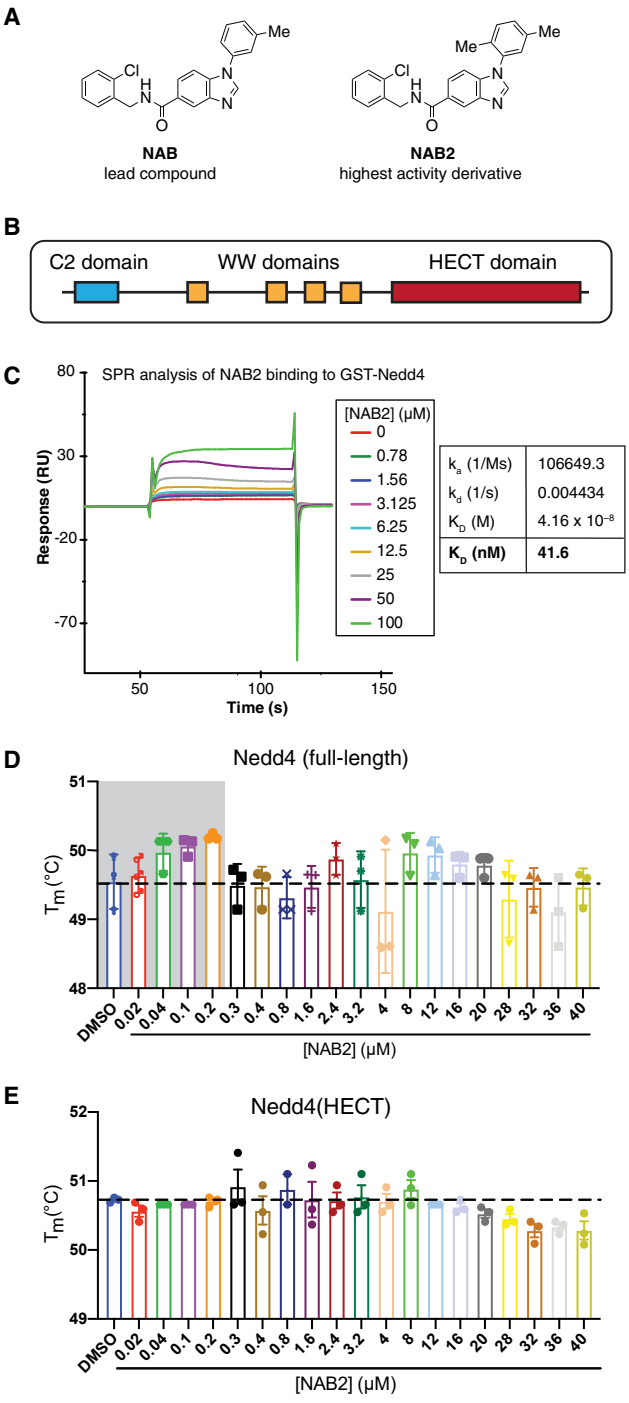

Figure 1. *In Vitro* Analyses Demonstrate NAB2 Engagement with Nedd4

(A) Phenotypic screening and SAR optimization identified a lead compound of an N-arylbenzdiimidazole scaffold (NAB; 40% effective concentration [EC_{40}] = 7.5 μM) and improved derivative NAB2 (EC_{40} = 4.5 μM) which significantly alleviated markers of α-synuclein toxicity.

(B) Linear representation of full-length Nedd4 depicts the subdomains of Nedd4. The enzyme contains a C2 domain (cyan) for membrane localization, four WW domains (yellow) for substrate recognition, and a catalytic HECT domain (red).

(C) Characterization of NAB2 binding by surface plasmon resonance (SPR) show that NAB2 binds to GST-Nedd4 with an apparent affinity of 41.6 nM relative to a control surface.

(D and E) Protein thermal shift assays (PTSAs) were conducted using SYRPO orange detection of Nedd4 stability after NAB2 treatment. PTSA analysis shows (D) an NAB2-dependent change in full-length Nedd4 stability at nanomolar concentrations (highlighted in gray) but is not reflective of a single binding event, whereas in (E), Nedd4(HECT) showed no significant change. Data shown as mean ± SEM of triplicate measurements.

2011). Furthermore, Nedd4 ubiquitinates aggregated α-synuclein more extensively than monomeric α-synuclein, indicating that it has potential to be specifically involved in clearance of the toxic proteoform (Mund et al., 2018). Nedd4 has also been implicated in cellular responses to stressors, including heat shock, oxidative stress, and protein misfolding (Fang et al., 2014; Kwak et al., 2012; Sommer et al., 2014). As α-synuclein-associated toxicity is a result of both protein aggregation and induced oxidative stress, the implication of Nedd4 in the response to α-synuclein-specific toxicity is promising.

Despite the role of Nedd4 in response to toxicity, the enzyme is considered a non-canonical drug target due to its lack of discrete active site and complex enzymatic mechanism. As a HECT-type E3 ubiquitin ligase (Figure 1B), Nedd4 depends upon protein-protein interactions with the upstream E2-conjugating enzyme and downstream substrate. It requires two chemical steps: transthioesterification for receipt of ubiquitin from the E2, and isopeptide bond formation for passage of ubiquitin to the substrate. Despite this, as an E3 ligase Nedd4 directly interacts with substrates and thus confers the greatest specificity for chemical manipulation of ubiquitination. While there is some precedence for small-molecule inhibition or alteration of Nedd4 activity or processivity (Chen et al., 2018; Kathman et al., 2015; Mund et al., 2014), ligands identified to date that specifically target the ligase are primarily covalent modifiers, and the ability to target Nedd4 with non-covalent ligands remains underexplored. We therefore sought to interrogate the NAB mechanism to better understand its impact on the activity and specificity of Nedd4, specifically as it pertains to α-synuclein toxicity.

Preliminary characterization of the mechanism of NABs indicates that, while activity is dependent upon Rsp5/Nedd4 and treatment with NAB decreased aggregate formation, it did not induce significant degradation of α-synuclein (Chung et al., 2013; Tardiff et al., 2013). In addition, NAB treatment did not inhibit Rsp5/Nedd4-dependent ubiquitination *in vitro*. Despite this, a single point mutation in Rsp5 abolished NAB activity (Tardiff et al., 2013). We hypothesize that NAB may modulate Nedd4 activity (i.e., kinetics or ubiquitin linkage specificity), or may alter its substrate specificity, thereby influencing Nedd4-dependent target ubiquitination and impacting downstream toxicity signaling events. To interrogate these hypotheses, we used *in vitro* biochemical and biophysical analyses in combination with cellular and proteomic experiments to characterize the mechanism of Nedd4 in response to NAB2 treatment. Here, we present the results of these analyses, which indicate that NAB2 engages with Nedd4 with apparent nanomolar affinity but does not induce changes in Nedd4 activity, conformation, or ubiquitin linkage specificity *in vitro*. At a cellular level, microscopy-based co-localization studies show the NAB2 mechanism is largely independent of Nedd4 localization changes. Through proteomic analyses, we demonstrate that α-synuclein toxicity drastically remodels the ubiquitylome with significant toxicity-dependent alterations in

ubiquitination of proteins related to gene expression, protein synthesis, and metabolic processes. Furthermore, we identify that NAB2 treatment induces significant changes in ubiquitination of transport-associated proteins relative to control samples. In particular, we identify a Nedd4 substrate, TFG, that serves as a regulatory protein in endoplasmic reticulum (ER)-to-Golgi trafficking and is ubiquitinated in an NAB2-dependent manner in cellular models of α-synuclein toxicity. Together, these experiments demonstrate that NAB2 engages with Nedd4 and implicates Nedd4 in NAB2-dependent changes in ER-to-Golgi transport, providing insight into (1) the Nedd4/NAB2 interaction, (2) the cellular effects of α-synuclein toxicity and the NAB2 mechanism in the rescue thereof, and (3) a putative trafficking protein network implicated in NAB2 treatment.

RESULTS

Surface Plasmon Resonance and Protein Thermal Shift Assays to Characterize NAB2 Binding to Nedd4

Initial characterization of NAB2 revealed that its activity was dependent upon Rsp5 or homolog Nedd4 in yeast and mammalian models, respectively (Chung et al., 2013; Tardiff et al., 2013). Therefore, we first sought to characterize the on-target binding of NAB2 through *in vitro* analyses. To quantify the affinity of NAB2 to Nedd4, ligand binding was characterized through surface plasmon resonance (SPR) using GST-Nedd4. SPR analysis of binding relative to a control surface indicated that NAB2 bound to GST-Nedd4 with an apparent K_D (K_D^{app}) of 41.6 nM (Figure 1C). Further analysis by SPR of ligand binding to the isolated catalytic HECT domain, a stable subdomain of the full-length ligase, did not show a canonical binding curve (Figure S1A). This result indicates that NAB2 binding is presumably occurring upstream of the C terminus catalytic HECT domain. To further validate binding analyses and to investigate the stoichiometry of the NAB2/Nedd4 interaction, we turned to isothermal titration calorimetry (ITC). Using ITC, no binding event was detected upon titration of NAB2 into the Nedd4(HECT) domain (Figure S1B), validating SPR results. ITC analysis of full-length Nedd4 was unsuccessful as the full-length protein suffered from instability and precipitation during extended ITC titrations (Figure S1C), so we instead used a protein thermal shift assay (PTSA) to further characterize ligand binding to Nedd4 (Figure 1D). PTSA analyses reveal an NAB2-dependent shift in the T_m of full-length Nedd4 at nanomolar concentrations, indicating a ligand-dependent change in protein stability. While this result is consistent with the K_D^{app} determined by SPR, the thermal shift results at higher NAB2 concentrations are not consistent with a 1:1 binding event as there is no direct concentration-dependent thermodynamic shift across the full range of NAB2 concentrations tested. Instead, the result indicates that a more complex binding event may be occurring. PTSA analysis of NAB2-induced changes in Nedd4(HECT) thermostability are consistent with SPR and ITC results (Figure 1E). Cumulatively, *in vitro* analyses of target engagement demonstrate that NAB2 binds to Nedd4 with high apparent affinity upstream of the HECT domain.

Bottom-up Hydrogen-Deuterium Exchange Mass Spectrometry Enables Characterization of Ligand-Induced Conformational Changes

We next sought to characterize the ligand binding site and any NAB2-dependent conformational changes induced by NAB2 binding to Nedd4. This is particularly important in the case of Nedd4 as its enzymatic activity is governed by regulatory intramolecular interactions (Chen et al., 2017; Jiang et al., 2019; Mari et al., 2014; Plant et al., 1997; Wang et al., 2010); thus, ligand-induced conformational changes may have functional implications. To characterize effect of NAB2 on Nedd4 conformation or flexibility, we used bottom-up hydrogen-deuterium exchange mass spectrometry (HDX-MS) (Kan et al., 2013) as there is precedence for the use of HDX-MS for characterization of protein-ligand complexes, particularly for ligands that induce conformational changes (Huang et al., 2011; Wang et al., 2017; Zhu et al., 2003).

We hypothesized that if NAB2 binding shields the Nedd4 backbone we would detect a localized change in deuterium uptake. Furthermore, if NAB2 treatment alters Nedd4 conformation by altering the relative order of the enzyme or changing intramolecular interactions between Nedd4 subunits, the ligand-induced change could be detected by a change in the rate of deuterium uptake relative to a DMSO-treated control. To this end, HDX-MS analysis was conducted using recombinant, full-length Nedd4 in the presence of NAB2 or DMSO control (Figure 2). Before time course analysis, peptide coverage of the protein sequence was confirmed, revealing that pepsin digestion provided high coverage across the length of Nedd4 (Figure 2B). An HDX time course experiment was conducted at time points ranging from 10 s to 3 h to enable exchange to occur in both disordered and ordered regions of the protein (Figures 2A, 2C, and S2). HDX data were collected at every time point for 752 of 900 residues, covering 83.5% of the total Nedd4 sequence. The results of bottom-up HDX-MS indicate that Nedd4 conformation is consistent with the relative order of the protein as predicted by the Predictor of Naturally Disordered Regions (PONDR) algorithm (Figure 2A; www.pondr.com) wherein more ordered regions of Nedd4 (N-terminal C2 domain and C-terminal HECT domain) did not uptake deuterium as rapidly as disordered linker regions. While the rate of deuterium uptake corresponds well with the predicted order of the Nedd4 structure (Figure 2C, top), the results show that NAB2 treatment (Figure 2C, middle) did not induce a significant global difference in the rate of deuterium uptake relative to the DMSO control (Figure 2C, bottom). This result indicates that NAB2 treatment does not induce a global change in Nedd4 conformation. It is important to note that a significant portion of the protein (between the C2 and HECT domain, encompassing the WW domains and linker regions) was partially or fully deuterated even at the shortest time point of the HDX-MS time course experiment. If NAB2 induces a conformational change in this region, it would not be easily detected due to limitations in the sensitivity of the method used unless the change resulted in significant shielding. We did, however, observe slight alterations in deuterium uptake in the C2, linker, and WW domain 2. This result is consistent with NAB2 binding upstream of the C-terminal HECT domain, but further investigation of the NAB2 binding mode is needed and will be explored in future analyses. Cumulatively, the results from HDX-MS and measurements of NAB2 binding show that NAB2 binding does not alter Nedd4 conformation *in vitro*.

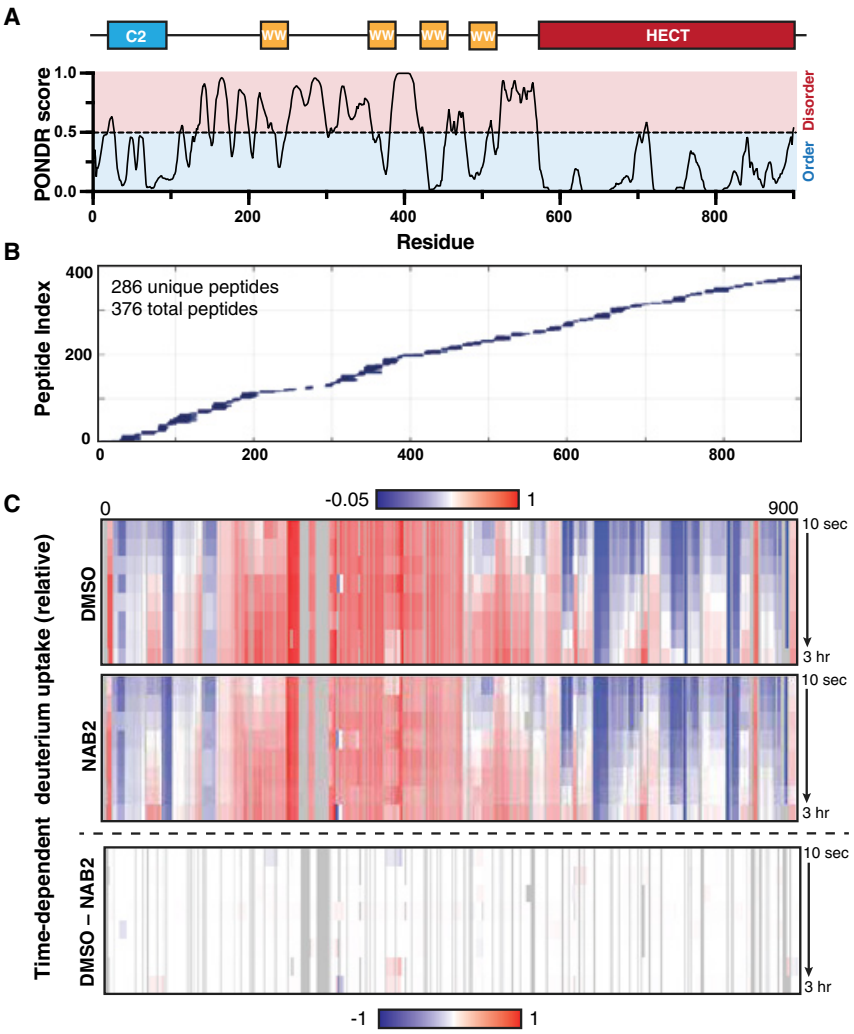

Figure 2. HDX-MS Shows No Significant Ligand-Induced Changes in Nedd4 Conformation

(A) The relative order of the protein was predicted with the PONDR algorithm (www.pondr.com) and corresponds well with the subdomains of the ligase structure (top).

(B) Peptide coverage map of full-length Nedd4 shows that diagnostic pepsin digest gave high coverage of the sequence for HDX analysis.

(C) Nedd4 conformation was mapped by HDX-MS in the presence of NAB2 or DMSO control. The rate of deuterium uptake into the Nedd4 backbone over time was consistent with the predicted order of the protein (top), compared with (A). NAB2 treatment (middle) did not induce a significant conformational change relative to a DMSO-treated control as indicated by little difference in the subtraction map (bottom).

Quantitative MALDI-TOF and Immunoblotting Assays for Measurement of NAB2-Induced Changes in Nedd4 Activity

The initial characterizations of NAB2 by *in vitro* immunoblotting assays suggested that it did not inhibit Nedd4 activity (Tardiff et al., 2013). It was not determined, however, if NAB2 treatment altered Nedd4 kinetics or ubiquitin linkage specificity, so we sought to characterize NAB2-dependent changes of Nedd4 enzymology more thoroughly. To assay Nedd4 activity in a sensitive, quantitative manner, we adapted a MALDI-TOF ubiquitination assay that measures monoubiquitin consumption over time relative to an internal standard (De Cesare et al., 2018) (Figures 3A and 3B). Analysis of relative Nedd4 activity showed that NAB2 treatment did not significantly alter the rate of monoubiquitin consumption by the full-length ligase *in vitro* (Figure 3C), suggesting that NAB2 does not alter the kinetics of Nedd4-dependent ubiquitination.

We next interrogated the linkage specificity of ubiquitin chains assembled by Nedd4. Nedd4 has been previously shown to assemble K48- and K63-linked ubiquitin chains as its primary products (Sugeno et al., 2014). We sought to determine if NAB2 treatment altered Nedd4 linkage specificity and, subsequently, the fate of Nedd4 substrates. Using an *in vitro* ubiquitination assay, we detected no difference in the formation of K48- or K63-linked chains after NAB2 treatment relative to DMSO control (Figures S3 and 3D). The lack of NAB2-dependent alteration of Nedd4 kinetics or ubiquitin linkage specificity *in vitro* suggested that a cellular model would be needed to uncover a potential mechanism of action (MOA).

Confocal Immunofluorescence Microscopy to Map NAB2-Dependent Changes in Nedd4 Localization

Nedd4 activity is tightly regulated (Chen et al., 2017; Jiang et al., 2019; Mari et al., 2014; Wang et al., 2010) and is dependent upon protein-protein interactions with its upstream E2-conjugating enzyme and downstream substrate. Since NAB2 did not affect Nedd4 activity *in vitro*, we hypothesized that it may instead rescue interactions between Nedd4 and proteins involved in trafficking (processes disrupted by α-synuclein toxicity). To determine if this occurs as a function of Nedd4 localization, we first used subcellular fractionation to quantify the distribution of Nedd4 across compartments and determined that NAB2 treatment does not alter the subcellular compartmentalization of Nedd4 (Figure S4). We then used confocal microscopy to visualize the co-localization of Nedd4 with Rab5a, GLG1, and calreticulin as markers of endosomes, Golgi apparatus, and ER, respectively (Figure 4B). In this experiment, we sought to determine the degree of Nedd4 co-localization with trafficking organelles at basal levels and in response to NAB2 treatment. We hypothesized that NAB2-dependent recruitment of Nedd4 to trafficking organelles would be indicated by an increase in co-localization of Nedd4 with trafficking organelle markers, thereby providing a possible mechanistic explanation for Nedd4 ubiquitination of trafficking proteins in an NAB2-dependent manner. To this end, we conducted confocal microscopy analyses of Nedd4 co-localization with trafficking markers as measured by Pearson's correlation coefficient (PCC). The confocal analysis suggested that Nedd4

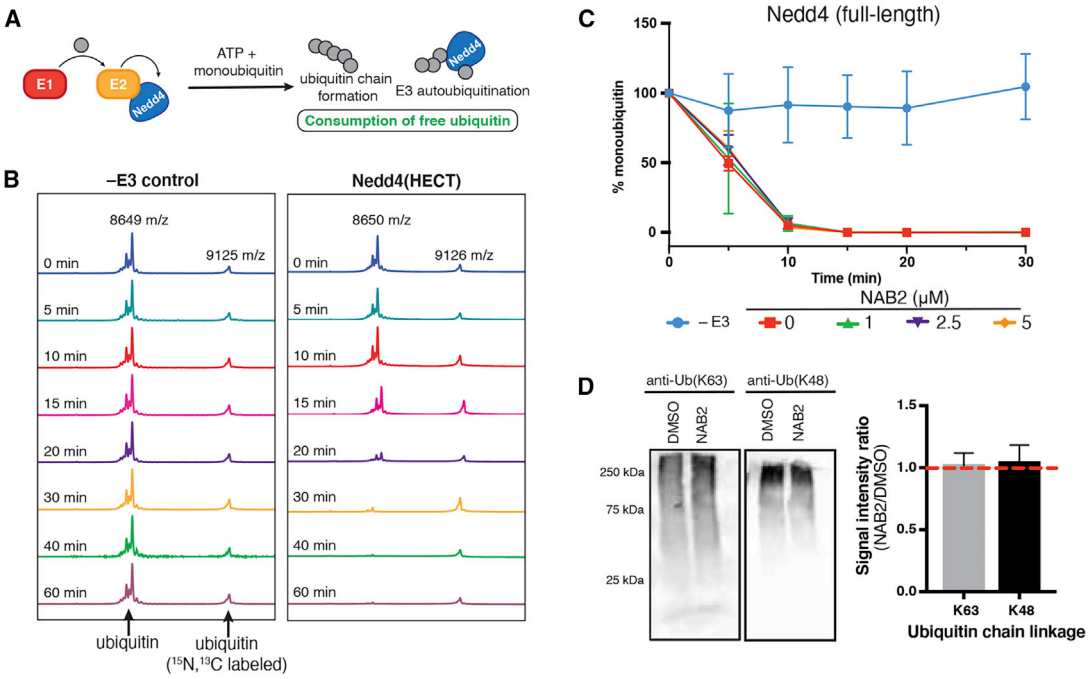

Figure 3. NAB2 Treatment Does Not Alter Nedd4 Activity or Conformation

(A) *In vitro* analysis of E3 ligase activity can be monitored by consumption of monoubiquitin (detected via MALDI-TOF and quantified relative to an internal standard).

(B) Representative MALDI-TOF traces show monoubiquitin consumption by Nedd4(HECT).

(C) Quantitative MALDI-TOF analysis shows no significant change in the rate of full-length Nedd4-dependent monoubiquitin consumption in the presence of NAB2 relative to a DMSO control. Data shown as average of triplicate ± SEM.

(D) Endpoint *in vitro* assays of Nedd4 activity allow for immunoblotting detection of Nedd4-dependent ubiquitin chain linkage specificity. *In vitro* specificity of chain linkage is not altered by NAB2 treatment relative to DMSO control. A representative blot is provided (full blots in Figure S3), and data are shown as average of triplicate ± SEM.

exhibits moderate co-localization with trafficking markers in untreated samples (Figure 4; as indicated by a positive PCC). Comparison of PCC values for NAB2-treated samples showed that the co-localization of Nedd4 with trafficking markers increased slightly after NAB2 treatment, with a significant change in co-localization only occurring with Rab5a (Figure 4B). These results indicate that NAB2 treatment does not significantly alter the co-localization of Nedd4 with the ER and Golgi despite the fact that NAB2 rescues ER-to-Golgi transport, thus eliminating NAB2-dependent changes in Nedd4 localization as an explanation of the NAB2 MOA.

Ubiquitin Enrichment-Coupled Proteomic Analyses for Assessment of NAB2-Dependent Changes in the Ubiquitylome

As NAB2 did not alter Nedd4 activity *in vitro* or Nedd4 co-localization with the ER/Golgi system, we hypothesized that it may instead alter the specificity of Nedd4, which could be reflected by changes in the global ubiquitylome. As a proof-of-concept screen, we used a tandem ubiquitin binding entity (TUBE) enrichment approach coupled to liquid chromatography-tandem mass spectrometry (LC-MS/MS) to investigate the ubiquitylome in response to time-dependent NAB2-treatment versus a DMSO control (Figure 5A). Qualitative proteomic characterization of NAB2-dependent changes in the total ubiquitylome identified 2,841 total proteins across all samples (Figure S5A). Within this pool, 532 unique, non-redundant proteins were found to be enriched in the ubiquitylome only after NAB2 treatment (across all time points). This subset of proteins qualitatively indicates that NAB2 treatment alters the ubiquitylome and supports our hypothesis that NAB2-induced changes in Nedd4 specificity could be reflected at the level of the global ubiquitylome. Interestingly, functional annotation of the enriched ubiquitylome via the PANTHER (Mi et al., 2005; Mi and Thomas, 2009) classification system indicates that the proteins present in the NAB2-dependent sub-ubiquitylome contain a higher proportion of trafficking-associated proteins compared with the total ubiquitylome or DMSO control (Figures S5B and S5C). The qualitative analysis thus provided proof-of-concept results that informed the design of subsequent quantitative experiments.

To better model the pathophysiological conditions that are rescued by NAB2, we applied this approach to quantify changes in protein ubiquitination in an NAB2-dependent manner. To this end, we conducted quantitative analyses of TUBE-enriched ubiquitylomes of both WT SHSY5Y cells and in SHSY5Y cells overexpressing A53T α-synuclein, a mutant form of α-synuclein that has been shown to induce protein aggregation and trafficking defects (Cooper et al., 2006). We also included an additional control, NAB17, an NAB analog identified in the original SAR study as a phenotypically inactive derivative (Figure 5B)

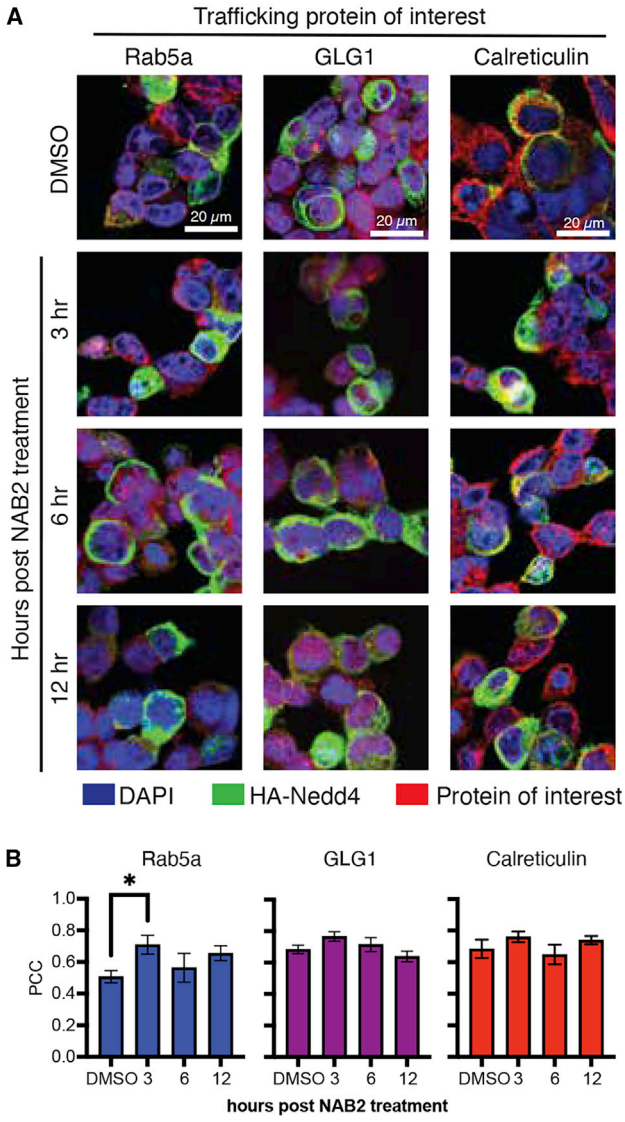

Figure 4. Localization Experiments Enable Measurement of Nedd4 Co-localization with Trafficking Organelles

Confocal immunofluorescence microscopy was used to measure the degree of Nedd4 co-localization with trafficking organelle markers at basal levels and following NAB2 treatment in SHSY5Y cells. Analyses revealed moderate co-localization of HA-Nedd4 with Rab5a, GLG1, and calreticulin, well-established protein markers of the endosome, Golgi, and endoplasmic reticulum, respectively. Time-dependent NAB2 treatment shows slight increases in Nedd4 localization with the trafficking organelle markers with a significant change only present at 3 h after NAB2 treatment in the Rab5a sample. Co-localization was measured volumetrically (across all slices of a z stack) in single cells (defined as regions of interest) and quantified using Pearson's correlation coefficient (PCC) wherein a more positive PCC value indicates a higher degree of co-localization. Representative images (A) are shown and PCC data (B) are shown as average PCC ± SEM of a minimum of 15 single cells across three microscopy frames. Statistical significance was calculated with an unpaired t test comparing NAB2 samples with DMSO control. For all samples, there is no significant difference unless specifically denoted where *$p < 0.05$. Image analysis was conducted with Imaris and data analysis in Prism (GraphPad).

(Tardiff et al., 2013). For the quantitative proteomics experiments, SHSY5Y (WT or α-synuclein-A53T overexpressing) cells were subsequently treated with DMSO, NAB2, or NAB17 before TUBE enrichment and label-free quantitative LC-MS/MS (Figure 5A). In total, 2,303 proteins were confidently quantified by 2 or more unique peptides across all replicates.

We anticipated that α-synuclein toxicity would significantly alter the ubiquitylome as part of the cellular response to the stress stimulus and that the effect of NAB2 on ER-to-Golgi trafficking may differ in the presence of α-synuclein toxicity relative to WT cells. To test these hypotheses, we first compared the effect of α-synuclein-A53T overexpression on the ubiquitylome relative to WT cells (Figure 5C). In this case, 385 proteins in the ubiquitylome (~17% of the total 2,303 quantified) were significantly altered in cells expressing α-synuclein-A53T relative to WT cells. GO enrichment (Eden et al., 2009) shows that α-synuclein toxicity enriches ubiquitination of proteins associated with gene expression, protein synthesis, and metabolic processes relative to the total ubiquitylome (Table S3). These results are consistent with previous characterizations of processes disrupted by α-synuclein-associated ER and cellular stress (Cheng et al., 2018; Eisbach and Outeiro, 2013; Fernandes et al., 2016; Jiang et al., 2010; Lautenschläger et al., 2017; Mercado et al., 2013; Zambon et al., 2019). Further analysis of ubiquitin linkage abundances (determined by comparison of diagnostic GG-K peptide abundances between samples) revealed that induction of α-synuclein toxicity increases the amount of K6-, K11-, K33-, K48-, and K63-linked ubiquitin chains relative to WT controls (Figure 5D). Strikingly, K63 linkages, which primarily trigger endocytosis and lysosomal degradation of plasma membrane proteins (Komander and Rape, 2012), are enriched 8-fold relative to the WT sample. Nedd4 assembles K63 chains as a primary product (Kim and Huibregtse, 2009) and has been well established to be involved in the response to α-synuclein toxicity; thus, it is feasible that Nedd4 is involved in the increase in K63 chains observed in this investigation. To further investigate the role of Nedd4 in the response to α-synuclein-induced changes in the ubiquitylome, we cross-referenced the total quantitative proteomics dataset with a compiled Nedd4 interactome (see STAR Methods), revealing 104 known Nedd4 substrates in the ubiquitylome and only 5 previously annotated substrates in the α-synuclein-dependent hits (Table S4). This result indicates that the Nedd4 interactome is potentially largely underexplored, particularly in regard to how its interactions are altered by cellular stimuli such as α-synuclein toxicity.

To complement *in vitro* analyses of the NAB2 mechanism described above, we first analyzed the effect of NAB2 treatment on GG-K peptide abundances (Figure 5D). NAB2-treated α-Syn-A53T OE cells show a decrease in K63 ubiquitination relative to DMSO-treated cells, indicating that there is an NAB2-dependent shift in the ubiquitylome. To identify specific proteins potentially involved in the NAB2-dependent network, we next compared the effect of NAB2 treatment in α-synuclein toxic cells (α-Syn-A53T OE SHSY5Y) relative to DMSO- and NAB17-treated controls (Figure 5E). Comparison of NAB2-treated samples shows significant alteration of 12 and 45 proteins in the ubiquitylome relative to the DMSO and NAB17 controls, respectively. Cross-reference of the significant hits identified by comparison with DMSO- and NAB17-control samples reveals four proteins identified in both

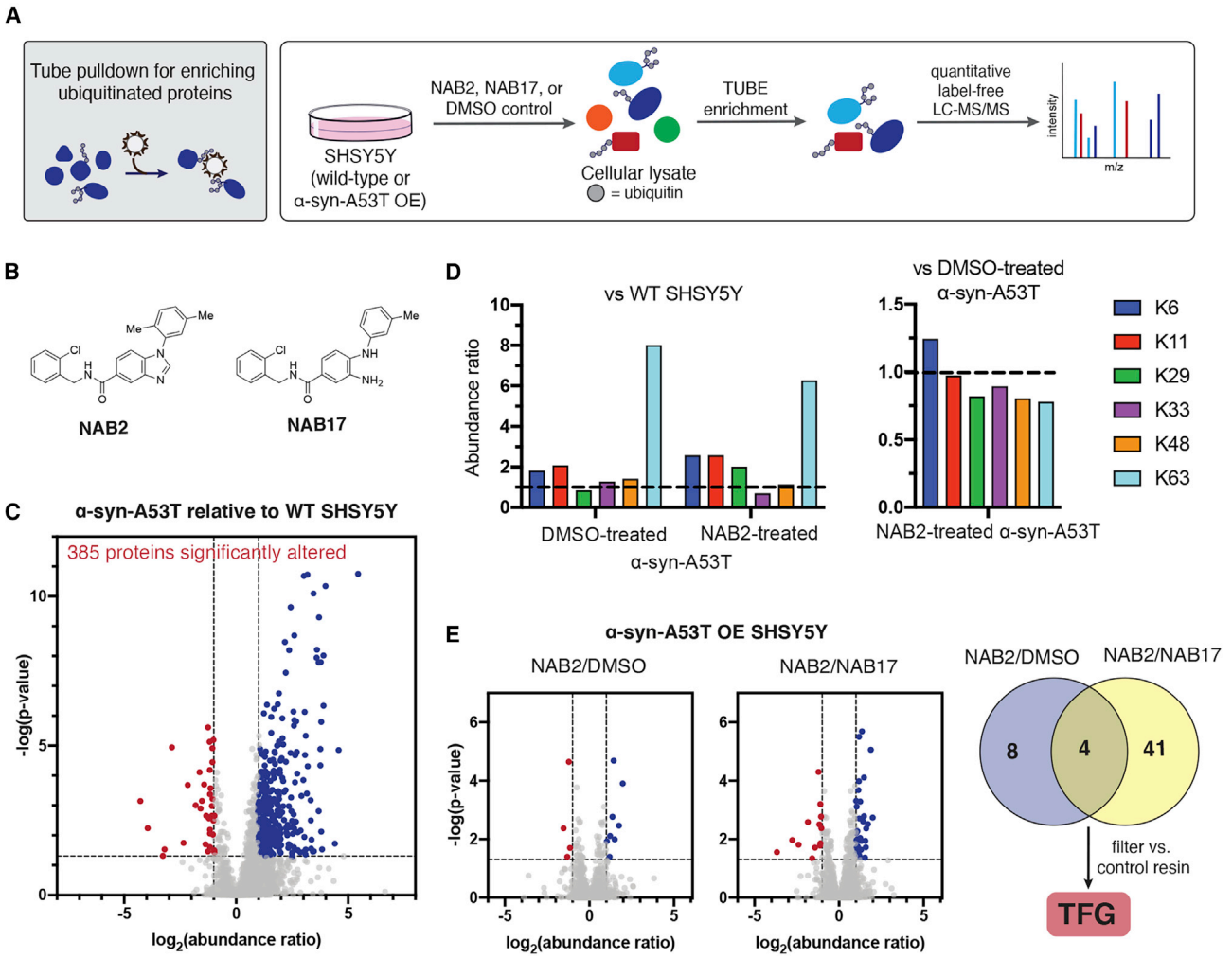

Figure 5. Proteomic Analysis of the Global Ubiquitylome Reveals α-Synuclein- and NAB2-Dependent Changes in Trafficking Protein Ubiquitination

(A) Ubiquitinated proteins were enriched from WT or α-synuclein-A53T-overexpressing SHSY5Y cells treated with NAB2, NAB17, or DMSO control. Following treatment, lysates were processed by pan-specific TUBE pull-down. Ubiquitinated proteins were characterized by proteolysis-coupled LC-MS/MS and quantitative abundance changes were measured across three replicates.

(B) Structure of NAB2 and NAB17, a phenotypically inactive NAB used as a second control.

(C) α-Synuclein overexpression induces dramatic changes in the ubiquitylome relative to WT SHSY5Y cells (significance determined using ± 2-fold change and $p < 0.05$ cutoffs).

(D) α-Synuclein overexpression alters the ubiquitylome at the level of ubiquitin linkage prevalence. NAB2 treatment decreases the ratio of K63 linkage relative to untreated α-Syn-A53T OE. Ratios calculated from normalized peptide abundances across three biological replicates in quantitative mass spectrometry analysis.

(E) NAB2 treatment of α-Syn-A53T OE SHSY5Y cells provides 12 and 45 significant hits relative to DMSO and NAB17 controls, respectively, with 4 hits identified across both control samples. Further filtering by comparison with a negative control resin pull-down reveals one remaining hit protein, TFG.

control experiments (Figure 5E, right). To ensure that the identified hits were enriched with high specificity during the TUBE pull-down, we further filtered by comparison of abundance ratios in DMSO-treated α-Syn-A53T OE SHSY5Y relative to a negative control resin pull-down (using ± 2-fold change and $p < 0.05$ cutoffs). With this additional filter, TFG is the only remaining hit protein. TFG has been previously reported as a substrate of ubiquitination (Beltrao et al., 2012; Povlsen et al., 2012; Rose et al., 2016; Sarraf et al., 2013; Stes et al., 2014; Udeshi et al., 2012; Wagner et al., 2011), so to better understand if it was a potential Nedd4 substrate, we turned to bioinformatic analyses of its primary protein sequence and interactome. Nedd4 contains four WW domains that recognize substrates that contain proline-rich PY motifs (e.g., PPxY, LPxY) or proteoforms that contain phosphothreonine (pT) or phosphoserine (pS) residues. TFG contains several proline-proline dipeptides and a QPPY sequence but not a canonical PY motif. There is evidence of TFG phosphorylation, with multiple reports of pT or pS proteoforms (Amanchy et al., 2008; Bian et al., 2014; Persaud et al., 2014; Sharma et al., 2014). Despite this, analysis of the Nedd4 interactome reveals that TFG has not been annotated as a Nedd4 interactor. To determine if TFG is ubiquitinated by

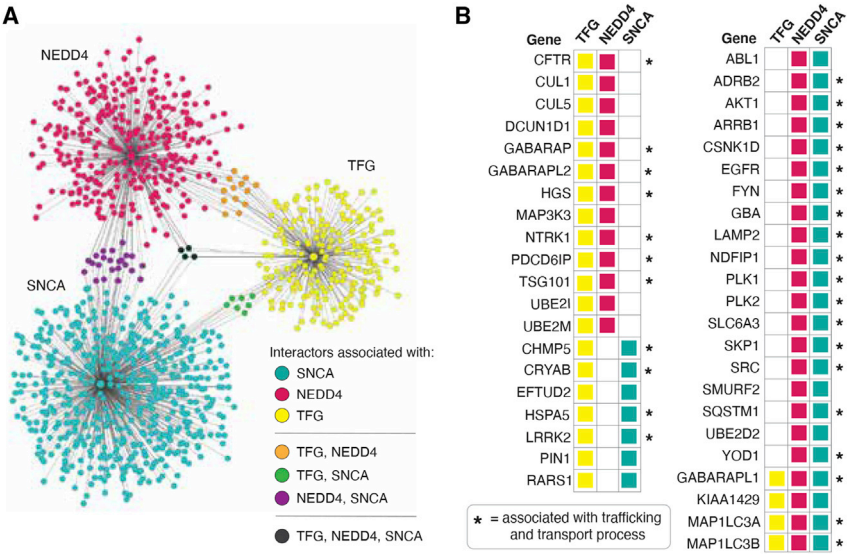

Figure 6. Analysis of Hits Identified in Quantitative Identification of NAB2-Dependent Ubiquitylome

(A) Merged protein-protein interaction networks from the IntAct and BioGrid databases show interactors of TFG, α-synuclein, and Nedd4. Networks visualized using Cytoscape (Shannon et al., 2003).

(B) Functional annotation reveals trafficking processes as links between proteins. The networks in which each shared protein are found are indicated by colors corresponding with the legend in (A).

Nedd4, we used an *in vitro* immunoblotting-based ubiquitination assay. Chemiluminescence detection reveals stronger signals at molecular weights higher than that of unmodified TFG (43 kDa) in the presence of Nedd4 relative to –Nedd4 control (Figure S6). This result is indicative of Nedd4-dependent ubiquitination of TFG, although it should be noted that there was a significant amount of unmodified TFG even with an extended assay duration (3 h) and excess ubiquitin. This indicates that TFG is a weak substrate of Nedd4 or that Nedd4 recognition of TFG requires specific TFG proteoforms (pT, pS), which may not be predominant in the lysate sample. Alternatively, the rate of Nedd4 ubiquitination of TFG may be altered by Nedd4 post-translational regulation, a condition that is not captured by the use of recombinant Nedd4.

With the role of Nedd4 and NAB2 treatment in rescuing α-synuclein-associated trafficking defects in mind, we sought to further understand the potential role of TFG in this process through functional and interaction network analyses. Excitingly, TFG is involved in the regulation of ER-to-Golgi trafficking (Beetz et al., 2013; Kanadome et al., 2017; Witte et al., 2011), the process that is disrupted by α-synuclein toxicity and rescued by NAB2 treatment. Specifically, TFG has been annotated as a scaffolding protein, with a putative coiled coil structure that drives self-oligomerization as well as protein binding events required for the process of COPII-coated vesicle secretion from the ER (Beetz et al., 2013; Kanadome et al., 2017; Witte et al., 2011). To further understand the possible functional connections between TFG, Nedd4, and α-synuclein at a cellular level, we generated a merged interaction network of the experimentally annotated interactome of each of these proteins using Cytoscape (Figure 6A) (Shannon et al., 2003). Interestingly, there are several proteins that are shared between the interactomes of Nedd4, α-synuclein, and TFG (Figure 6). Functional annotation reveals that 13 of the 24 shared interactors are associated with trafficking and transport processes (Figure 6B), establishing a biological link between TFG, Nedd4, and α-synuclein. Of particular interest in the shared interactome are proteins, such as LRRK2 (a kinase that is well established for its role in a genetic form of PD) (Blanca Ramírez et al., 2017), GABARAP, GABARAPL1/GABARAPL2, as well as MAP1LC3A and MAP1LC3B. The latter five proteins are key regulators in autophagosome formation and maturation, and maintenance of cellular homeostasis (Wild et al., 2014). While we anticipate that other proteins, including those outside of the enriched ubiquitylome, may be involved in the NAB2-dependent rescue of ER-to-Golgi trafficking, the use of quantitative TUBE-coupled proteomics provides insight into the effect of both α-synuclein toxicity and NAB2 treatment on the ubiquitylome. Furthermore, bioinformatic analysis complements the proteomic results by revealing a putative protein network connecting the proteins of interest.

DISCUSSION

Initial identification of NAB2 as a potential anti-parkinsonian lead compound showed that its activity was dependent upon E3 ubiquitin ligase Nedd4 (Tardiff et al., 2013), but target engagement and biochemical validation of the NAB2 MOA was unexplored. Here, we present a biochemical and biophysical interrogation of NAB2 target engagement with Nedd4, a putative target identified through chemical genetic screening. We observed that NAB2 bound to Nedd4 with nM affinity (K_D^{app}) with binding occurring upstream of the C-terminal catalytic domain. *In vitro* analyses of Nedd4 activity reveal that NAB2 does not alter the global conformation, activity, or ubiquitin linkage specificity of Nedd4 as measured by bottom-up HDX-MS and quantitative activity assays. While HDX-MS results indicate that NAB2 does not induce a global conformational change, there are small regions in which deuterium uptake changes in an NAB2-dependent manner. These areas are distributed across the N-terminal end of the protein, a result which is consistent with our measurements of NAB2 binding in which NAB2 binds to full-length Nedd4 but not the isolated C-terminal HECT domain. Other *in vitro* analyses of Nedd4 activity and ubiquitin linkage specificity indicate no global NAB2-dependent change in the backbone conformation, but are consistent with a side-chain-mediated interaction that does not inhibit its E3 ligase activity, but most likely modulates its substrate specificity. It is important to note, however, that Nedd4 has many possible interactions with upstream E2 enzymes, downstream substrates, and regulatory proteins, which are likely dependent upon cellular stimuli (Yang and Kumar, 2010). Furthermore, Nedd4 activity can be

regulated by post-translational modifications that are not captured by *in vitro* analyses conducted with recombinantly purified enzyme (Chen et al., 2017; Persaud et al., 2014; Yang and Kumar, 2010). It is not sufficient, therefore, to only consider the results of *in vitro* analyses with limited interactors when defining the MOA of NAB2 as a modulator of Nedd4.

As NAB2 was shown to rescue ER-to-Golgi trafficking defects in a Nedd4-dependent manner, we turned to cellular and proteomic analyses to identify NAB2-dependent changes in Nedd4 localization with cellular trafficking machinery. Microscopy-based experiments show that Nedd4 exhibits moderate co-localization with the Golgi and ER at basal conditions and that NAB2 treatment induces slight but insignificant increases in Nedd4 localization with these organelles. Thus, Nedd4 localization is not altered in response to NAB2 treatment.

Subsequent proteomic interrogation of the ubiquitylome using TUBE-coupled proteomics indicates that α-synuclein toxicity drastically remodels the ubiquitylome, altering ubiquitination of proteins involved in processes previously reported to be disrupted by α-synuclein. Analysis of NAB2-treated α-synuclein toxic SHSY5Y cells revealed one significant hit relative to DMSO- and NAB17-treated controls. This hit, TFG, has been established as a regulator of ER-to-Golgi trafficking, the process that is disrupted by α-synuclein toxicity and restored by NAB2 treatment. While TFG has not been previously annotated as a Nedd4 substrate, our *in vitro* analyses demonstrate TFG ubiquitination in a Nedd4-dependent manner, establishing TFG as a Nedd4 substrate. Subsequent bioinformatic analysis of the TFG, α-synuclein, and Nedd4 interactomes reveal a network of functionally related, shared interactors as a putative network of trafficking proteins that link the NAB2-dependent hit with Nedd4 and α-synuclein. Furthermore, cross-reference of the Nedd4 interactome with proteomic hits shows that few proteins in the α-synuclein- or NAB2-dependent ubiquitylome are known Nedd4 interactors, indicating that the Nedd4 interactome is potentially largely underexplored. Thus, further analysis of Nedd4 interactions in the cell would provide insight into the role of the ligase in the rescue of α-synuclein toxicity.

Cumulatively, the analyses described here provide insight into the effects of α-synuclein toxicity and NAB2 treatment on the ubiquitylome and demonstrate that NAB2 binds to Nedd4 without altering its enzymatic activity or conformation *in vitro* and largely does not alter Nedd4 cellular localization relative to trafficking organelles. Our results indicate that NAB2 binding may induce a phenotypic alleviation of α-synuclein toxicity via a more complex mechanism. In complement, our proteomic characterization sheds light on the effects of α-synuclein toxicity on the ubiquitylome and related regulatory processes while revealing a Nedd4 substrate and putative protein network involved in NAB2-dependent restoration of trafficking defects. The efforts described advance our understanding of how α-synuclein aggregation disrupts homeostasis and of how NAB2 and Nedd4 are involved in the restoration thereof. Furthermore, our efforts highlight the power of phenotypic screens for the identification of novel ligands that can alter complex biological processes (like those associated with neurodegeneration) (Brown and Wobst, 2020) but also demonstrate that ligands identified in this manner may act via mechanisms that are not easily unraveled. While the use of these phenotype-driven platforms enables identification of active ligands, such as NAB2, there are many opportunities that remain in fully elucidating the mechanism by which NAB2 rescues α-synuclein toxicity. Specifically, we envision that further efforts toward (1) characterizing the NAB2 binding mode, (2) analyzing Nedd4 activity in cellular models in an NAB2-dependent manner, and (3) elucidating the interactome and specificity of Nedd4 in response to cellular stimuli will further advance our understanding of NAB2 as a therapeutic lead and of the role of Nedd4 in the alleviation of α-synuclein toxicity. Regardless, the efforts described here toward biochemical and proteomic validation provide valuable insight into possible NAB2 mechanisms and lay the groundwork for exciting biochemical investigations of NAB2 targets, Nedd4 specificity, and α-synuclein toxicity that are currently underway.

SIGNIFICANCE

Limitations in the long-term efficacy of PD therapeutics has motivated research to identify alternative drug targets and lead compounds. This process typically relies upon phenotype-driven screens for identification of compounds that can alleviate complex biological defects related to PD. While these approaches are powerful, they often identify lead compounds for which the specific cellular target or MOA is not known. To advance the compounds in therapeutic development, there is great utility in unraveling the underlying mechanisms. Here, we interrogate the mechanism of one such compound, NAB2, that was identified through phenotypic screening as a promising lead in the rescue of cellular toxicity in α-synuclein-associated models of PD. NAB2 was shown to rescue α-synuclein-associated trafficking defects, and its activity was dependent upon E3 ubiquitin ligase Nedd4 (Chung et al., 2013; Tardiff et al., 2013)**. We demonstrate that NAB2 binds to Nedd4 with high apparent affinity but does not alter its activity or conformation *in vitro*, suggesting that NAB2-induced changes in Nedd4 activity may be dependent upon cellular context and regulation. These biophysical and biochemical analyses are complemented by proteomic identification of NAB2-dependent changes in global protein ubiquitination through which we show that NAB2 stimulates the ubiquitination of trafficking-associated proteins. Our findings identify a Nedd4 substrate, TFG, which serves as a scaffolding protein in ER-to-Golgi trafficking, and a putative NAB2-dependent protein network involved in cellular trafficking. Furthermore, we demonstrate that the proteins affected by NAB2 are related to pathways altered in other forms of parkinsonian toxicity, and we anticipate that our findings lay the groundwork for further investigation of NAB2 specificity and translatability to other neurodegeneration-related trafficking defects.**

STAR★METHODS

Detailed methods are provided in the online version of this paper and include the following:

- KEY RESOURCES TABLE
- RESOURCE AVAILABILITY
  - Lead Contact

SUPPLEMENTAL INFORMATION

Supplemental Information can be found online at https://doi.org/10.1016/j.chembiol.2020.10.008.

ACKNOWLEDGMENTS

The authors kindly thank Dr. Brian Watts of the Duke Human Vaccine Institute for assistance with surface plasmon resonance experiments and Dr. Peter Silinski of the Duke Chemistry Shared Instrument Facility for assistance with the MALDI-TOF MS assay and HRMS. In addition, the authors also thank Addgene and depositors for access to plasmids. The authors acknowledge the Duke School of Medicine and the Duke Cancer Institute for the funding of the Lumos mass spectrometer used for proteomics analyses. Finally, the authors gratefully thank the members of the McCafferty lab for thoughtful feedback during the course of this project and in preparation of this manuscript.

Funding: This work was kindly supported by Duke University, NIH Grant 1R21NS112927-01 to D.G.M., Michael J. Fox Foundation Grant 16250 to D.G.M., National Science Foundation Grant MCB1020649 to S.W.E., and National Science Foundation Graduate Research Fellowship GRFP 2017248946 to A.K.H.

AUTHOR CONTRIBUTIONS

D.G.M. supervised the work described here, secured funding, mentored A.K.H. and H.D.A., and aided in manuscript preparation and editing. A.K.H. participated in conceptualization and execution of all experiments, data collection and visualization, and prepared the manuscript. H.D.A. assisted in protein purification and with *in vitro* assays. L.M. and S.W.E. provided access to instrumentation and advised on experiment design and data analysis with HDX-MS experiments. M.W.F. and M.A.M. assisted in data collection and analysis for proteomic experiments.

DECLARATION OF INTERESTS

The authors have no conflicts of interests to declare.

Received: June 5, 2020
Revised: September 18, 2020
Accepted: October 19, 2020
Published: November 10, 2020

REFERENCES

Amanchy, R., Zhong, J., Molina, H., Chaerkady, R., Iwahori, A., Kalume, D.E., Grønborg, M., Joore, J., Cope, L., and Pandey, A. (2008). Identification of c-Src tyrosine kinase substrates using mass spectrometry and peptide microarrays. J. Proteome Res. *7*, 3900–3910.

Beetz, C., Johnson, A., Schuh, A.L., Thakur, S., Varga, R.-E., Fothergill, T., Hertel, N., Bomba-Warczak, E., Thiele, H., Nürnberg, G., et al. (2013). Inhibition of TFG function causes hereditary axon degeneration by impairing endoplasmic reticulum structure. Proc. Natl. Acad. Sci. U S A *110*, 5091–5096.

Beltrao, P., Albanèse, V., Kenner, L.R., Swaney, D.L., Burlingame, A., Villén, J., Lim, W.A., Fraser, J.S., Frydman, J., and Krogan, N.J. (2012). Systematic functional prioritization of protein posttranslational modifications. Cell *150*, 413–425.

Bian, Y., Song, C., Cheng, K., Dong, M., Wang, F., Huang, J., Sun, D., Wang, L., Ye, M., and Zou, H. (2014). An enzyme assisted RP-RPLC approach for in-depth analysis of human liver phosphoproteome. J. Proteomics *96*, 253–262.

Blanca Ramírez, M., Madero-Perez, J., Rivero-Rios, P., Martinez-Salvador, M., Lara Ordonez, A.J., Fernandez, B., Fdez, E., and Hilfiker, S. (2017). LRRK2 and Parkinson's disease: from lack of structure to gain of function. Curr. Protein Pept. Sci. *18*, 677–686.

Brown, D.G., and Wobst, H.J. (2020). Opportunities and challenges in phenotypic screening for neurodegenerative disease research. J. Med. Chem. *63*, 1823–1840.

Brzovic, P.S., Lissounov, A., Christensen, D.E., Hoyt, D.W., and Klevit, R.E. (2006). A UbcH5/ubiquitin noncovalent complex is required for processive BRCA1-directed ubiquitination. Mol. Cell *21*, 873–880.

Calderone, A., Castagnoli, L., and Cesareni, G. (2013). Mentha: a resource for browsing integrated protein-interaction networks. Nat. Methods *10*, 690–691.

Chen, D., Gehringer, M., and Lorenz, S. (2018). Developing small-molecule inhibitors of HECT-type ubiquitin ligases for therapeutic applications: challenges and opportunities. ChemBioChem *19*, 2123–2135.

Chen, Z., Jiang, H., Xu, W., Amzel, L.M., Gabelli, S.B., and Cole, P.A. (2017). A tunable brake for HECT ubiquitin ligases in brief. Mol. Cell *66*, 345–357.e6.

Cheng, J., Lu, Q., Song, L., and Ho, M.S. (2018). α-Synuclein trafficking in Parkinson's disease: insights from fly and mouse models. ASN Neuro *10*, 1–19.

Chung, C.Y., Khurana, V., Auluck, P.K., Tardiff, D.F., Mazzulli, J.R., Soldner, F., Baru, V., Lou, Y., Freyzon, Y., Cho, S., et al. (2013). Identification and rescue of -synuclein toxicity in Parkinson patient-derived neurons. Science *342*, 983–987.

Cooper, A.A., Gitler, A.D., Cashikar, A., Haynes, C.M., Hill, K.J., Bhullar, B., Liu, K., Xu, K., Strathearn, K.E., Liu, F., et al. (2006). α-Synuclein blocks ER-Golgi traffic and Rab1 rescues neuron loss in Parkinson's models. Science *313*, 324–328.

De Cesare, V., Johnson, C., Barlow, V., Hastie, J., Knebel, A., and Trost, M. (2018). The MALDI-TOF E2/E3 ligase assay as universal tool for drug discovery in the ubiquitin pathway. Cell Chem. Biol. *25*, 1–11.

Del Mar, C., Greenbaum, E.A., Mayne, L., Englander, S.W., and Woods, V.L., Jr. (2005). Structure and properties of alpha-synuclein and other amyloids determined at the amino acid level. Proc. Natl. Acad. Sci. U S A *102*, 15477–15482.

Eden, E., Navon, R., Steinfeld, I., Lipson, D., and Yakhini, Z. (2009). GOrilla: a tool for discovery and visualization of enriched GO terms in ranked gene lists. BMC Bioinformatics *10*, 48.

Eisbach, S.E., and Outeiro, T.F. (2013). alpha-Synuclein and intracellular trafficking: impact on the spreading of Parkinson's disease pathology. J. Mol. Med. *91*, 693–703.

Fang, N.N., Chan, G.T., Zhu, M., Comyn, S.A., Persaud, A., Deshaies, R.J., Rotin, D., Gsponer, J., and Mayor, T. (2014). Rsp5/Nedd4 is the main ubiquitin ligase that targets cytosolic misfolded proteins following heat stress. Nat. Cell Biol. *16*, 1227–1237.

Fernandes, H.J.R., Hartfield, E.M., Christian, H.C., Emmanoulidou, E., Zheng, Y., Booth, H., Bogetofte, H., Lang, C., Ryan, B.J., Sardi, S.P., et al. (2016). ER stress and autophagic perturbations lead to elevated extracellular α-synuclein in GBA-N370S Parkinson's iPSC-derived dopamine neurons. Stem Cell Reports *6*, 342–356.

Furlong, R.A., Narain, Y., Rankin, J., Wyttenbach, A., and Rubinsztein, D.C. (2000). alpha-Synuclein overexpression promotes aggregation of mutant huntingtin. Biochem. J. *346* (Pt 3), 577–581.

Gao, S., Alarcón, C., Sapkota, G., Rahman, S., Chen, P.-Y., Goerner, N., Macias, M.J., Erdjument-Bromage, H., Tempst, P., and Massagué, J. (2009). Ubiquitin ligase Nedd4L targets activated Smad2/3 to limit TGF-beta signaling. Mol. Cell *36*, 457–468.

Gitler, A.D., Bevis, B.J., Shorter, J., Strathearn, K.E., Hamamichi, S., Su, L.J., Caldwell, K.A., Caldwell, G.A., Rochet, J.-C., McCaffery, J.M., et al. (2008). The Parkinson's disease protein alpha-synuclein disrupts cellular Rab homeostasis. Proc. Natl. Acad. Sci. U S A *105*, 145–150.

Hatstat, A.K., and McCafferty, D.G. (2020). Robust and facile purification of full-length, untagged human Nedd4 as a recombinant protein from *Escherichia coli*. Protein Expr. Purif. *173*, 105649.

Hermjakob, H., Montecchi-Palazzi, L., Lewington, C., Mudali, S., Kerrien, S., Orchard, S., Vingron, M., Roechert, B., Roepstorff, P., Valencia, A., et al. (2004). IntAct: an open source molecular interaction database. Nucleic Acids Res. *32*, D452–D455.

Huang, R.Y.-C., Rempel, D.L., and Gross, M.L. (2011). HD exchange and PLIMSTEX determine the affinities and order of binding of Ca^{2+} with troponin C. Biochemistry *50*, 5426–5435.

Jiang, H., Thomas, S.N., Chen, Z., Chiang, C.Y., and Cole, P.A. (2019). Comparative analysis of the catalytic regulation of NEDD4-1 and WWP2 ubiquitin ligases. J. Biol. Chem. *294*, 17421–17436.

Jiang, P., Gan, M., Ebrahim, A.S., Lin, W.-L., Melrose, H.L., and Yen, S.-H.C. (2010). ER stress response plays an important role in aggregation of α-synuclein. Mol. Neurodegener. *5*, 56.

Jin, J., Li, X., Gygi, S.P., and Harper, J.W. (2007). Dual E1 activation systems for ubiquitin differentially regulate E2 enzyme charging. Nature *447*, 1135–1138.

Kan, Z.Y., Walters, B.T., Mayne, L., and Englander, S.W. (2013). Protein hydrogen exchange at residue resolution by proteolytic fragmentation mass spectrometry analysis. Proc. Natl. Acad. Sci. U S A *110*, 16438–16443.

Kan, Z.-Y., Ye, X., Skinner, J.J., Mayne, L., and Englander, S.W. (2019). ExMS2: an integrated solution for hydrogen–deuterium exchange mass spectrometry data analysis. Anal. Chem. *91*, 7481.

Kanadome, T., Shibata, H., Kuwata, K., Takahara, T., and Maki, M. (2017). The calcium-binding protein ALG-2 promotes endoplasmic reticulum exit site localization and polymerization of Trk-fused gene (TFG) protein. FEBS J. *284*, 56–76.

Kathman, S.G., Span, I., Smith, A.T., Xu, Z., Zhan, J., Rosenzweig, A.C., and Statsyuk, A.V. (2015). A small molecule that switches a ubiquitin ligase from a processive to a distributive enzymatic mechanism. J. Am. Chem. Soc. *137*, 12442–12445.

Kim, H.C., and Huibregtse, J.M. (2009). Polyubiquitination by HECT E3s and the determinants of chain type specificity. Mol. Cell. Biol. *29*, 3307–3318.

Komander, D., and Rape, M. (2012). The ubiquitin code. Annu. Rev. Biochem. *81*, 203–229.

Kwak, Y.D., Wang, B., Li, J.J., Wang, R., Deng, Q., Diao, S., Chen, Y., Xu, R., Masliah, E., Xu, H., et al. (2012). Upregulation of the E3 ligase NEDD4-1 by oxidative stress degrades IGF-1 receptor protein in neurodegeneration. J. Neurosci. *32*, 10971–10981.

Lashuel, H.A., Overk, C.R., Oueslati, A., and Masliah, E. (2013). The many faces of alpha-synuclein: from structure and toxicity to therapeutic target. Nat. Rev. Neurosci. *14*, 38–48.

Lautenschläger, J., Kaminski, C.F., and Kaminski Schierle, G.S. (2017). α-Synuclein—regulator of exocytosis, endocytosis, or both? Trends Cell Biol. *27*, 468–479.

Lesser, R.P., Fahn, S., Snider, S.R., Cote, L.J., Isgreen, W.P., and Barrett, R.E. (1979). Analysis of the clinical problems in parkinsonism and the complications of long-term levodopa therapy. Neurology *29*, 1253–1260.

Lynn, D.J., Winsor, G.L., Chan, C., Richard, N., Laird, M.R., Barsky, A., Gardy, J.L., Roche, F.M., Chan, T.H.W., Shah, N., et al. (2008). InnateDB: facilitating systems-level analyses of the mammalian innate immune response. Mol. Syst. Biol. *4*, 218.

Mari, S., Ruetalo, N., Maspero, E., Stoffregen, M.C., Pasqualato, S., Polo, S., and Wiesner, S. (2014). Structural and functional framework for the autoinhibition of Nedd4-family ubiquitin ligases. Structure *22*, 1639–1649.

Marsden, C.D., and Parkes, J.D. (1976). "On-off" effects in patients with Parkinson's disease on chronic levodopa therapy. Lancet *307*, 292–296.

Mercado, G., Valdés, P., and Hetz, C. (2013). An ERcentric view of Parkinson's disease. Trends Mol. Med. *19*, 165–175.

Mi, H., Lazareva-Ulitsky, B., Loo, R., Kejariwal, A., Vandergriff, J., Rabkin, S., Guo, N., Muruganujan, A., Doremieux, O., Campbell, M.J., et al. (2005). The PANTHER database of protein families, subfamilies, functions and pathways. Nucleic Acids Res. *33*, D284–D288.

Mi, H., and Thomas, P. (2009). PANTHER pathway: an ontology-based pathway database coupled with data analysis tools. Methods Mol. Biol. Clifton NJ *563*, 123–140.

Munchau, A., and Bhatia, K.P. (2000). Pharmacological treatment of Parkinson's disease. Postgrad. Med. J. *76*, 602–610.

Mund, T., Lewis, M.J., Maslen, S., and Pelham, H.R. (2014). Peptide and small molecule inhibitors of HECT-type ubiquitin ligases. Proc. Natl. Acad. Sci. U S A *111*, 16736–16741.

Mund, T., Masuda-Suzukake, M., Goedert, M., and Pelham, H.R. (2018). Ubiquitination of alpha-synuclein filaments by Nedd4 ligases. PLoS One *13*, e0200763.

Orchard, S., Kerrien, S., Abbani, S., Aranda, B., Bhate, J., Bidwell, S., Bridge, A., Briganti, L., Brinkman, F., Cesareni, G., et al. (2012). Protein interaction data curation: the International Molecular Exchange (IMEx) consortium. Nat. Methods *9*, 345–350.

Outeiro, T.F., Lindquist, S., Cashikar, A., Haynes, C.M., Hill, K.J., Bhullar, B., Liu, K., Xu, K., Strathearn, K.E., Liu, F., et al. (2003). Yeast cells provide insight into alpha-synuclein biology and pathobiology. Science *302*, 1772–1775.

Persaud, A., Alberts, P., Mari, S., Tong, J., Murchie, R., Maspero, E., Safi, F., Moran, M.F., Polo, S., and Rotin, D. (2014). Tyrosine phosphorylation of NEDD4 activates its ubiquitin ligase activity. Sci. Signal. *7*, ra95.

Pickart, C.M., and Raasi, S. (2005). Controlled synthesis of polyubiquitin chains. Methods Enzymol. *399*, 21–36.

Plant, P.J., Yeger, H., Staub, O., Howard, P., and Rotin, D. (1997). The C2 domain of the ubiquitin protein ligase Nedd4 mediates Ca^{2+}-dependent plasma membrane localization. J. Biol. Chem. *272*, 32329–32336.

Povlsen, L.K., Beli, P., Wagner, S.A., Poulsen, S.L., Sylvestersen, K.B., Poulsen, J.W., Nielsen, M.L., Bekker-Jensen, S., Mailand, N., and Choudhary, C. (2012). Systems-wide analysis of ubiquitylation dynamics reveals a key role for PAF15 ubiquitylation in DNA-damage bypass. Nat. Cell Biol. *14*, 1089–1098.

Riley, D.E., and Lang, A.E. (1993). The spectrum of levodopa-related fluctuations in Parkinson's disease. Neurology *8*, 1459–1464.

Rocha, E.M., De Miranda, B., and Sanders, L.H. (2018). alpha-Synuclein: pathology, mitochondrial dysfunction and neuroinflammation in Parkinson's disease. Neurobiol. Dis. *109*, 249–257.

Rose, C.M., Isasa, M., Ordureau, A., Prado, M.A., Beausoleil, S.A., Jedrychowski, M.P., Finley, D.J., Harper, J.W., and Gygi, S.P. (2016). Highly multiplexed quantitative mass spectrometry analysis of ubiquitylomes. Cell Syst. *3*, 395–403.e4.

Sarraf, S.A., Raman, M., Guarani-Pereira, V., Sowa, M.E., Huttlin, E.L., Gygi, S.P., and Harper, J.W. (2013). Landscape of the PARKIN-dependent ubiquitylome in response to mitochondrial depolarization. Nature *496*, 372–376.

Schindelin, J., Arganda-Carreras, I., Frise, E., Kaynig, V., Longair, M., Pietzsch, T., Preibisch, S., Rueden, C., Saalfeld, S., Schmid, B., et al. (2012). Fiji: an open-source platform for biological-image analysis. Nat. Methods *9*, 676–682.

Shannon, P., Markiel, A., Ozier, O., Baliga, N.S., Wang, J.T., Ramage, D., Amin, N., Schwikowski, B., and Ideker, T. (2003). Cytoscape: a software environment for integrated models of biomolecular interaction networks. Genome Res. *13*, 2498–2504.

Sharma, K., D'Souza, R.C.J., Tyanova, S., Schaab, C., Wiśniewski, J.R., Cox, J., and Mann, M. (2014). Ultradeep human phosphoproteome reveals a distinct regulatory nature of Tyr and Ser/Thr-based signaling. Cell Rep. *8*, 1583–1594.

Singleton, A.B., Farrer, M., Johnson, J., Singleton, A., Hague, S., Kachergus, J., Hulihan, M., Peuralinna, T., Dutra, A., Nussbaum, R., et al. (2003). α-Synuclein locus triplication causes Parkinson's disease. Science *302*, 841.

Sommer, T., Weber, A., and Jarosch, E. (2014). Rsp5/Nedd4 clears cells of heat-damaged proteins. Nat. Cell Biol. *16*, 1130–1132.

Stark, C., Breitkreutz, B.-J., Reguly, T., Boucher, L., Breitkreutz, A., and Tyers, M. (2006). BioGRID: a general repository for interaction datasets. Nucleic Acids Res. *34*, D535–D539.

Stes, E., Laga, M., Walton, A., Samyn, N., Timmerman, E., De Smet, I., Goormachtig, S., and Gevaert, K. (2014). A COFRADIC protocol to study protein ubiquitination. J. Proteome Res. *13*, 3107–3113.

Sugeno, N., Hasegawa, T., Tanaka, N., Fukuda, M., Wakabayashi, K., Oshima, R., Konno, M., Miura, E., Kikuchi, A., Baba, T., et al. (2014). Lys-63-linked ubiquitination by E3 ubiquitin ligase Nedd4-1 facilitates endosomal sequestration of internalized α-synuclein. J. Biol. Chem. *289*, 18137–18151.

Tardiff, D.F., Jui, N.T., Khurana, V., Tambe, M.A., Thompson, M.L., Chung, C.Y., Kamadurai, H.B., Kim, H.T., Lancaster, A.K., Caldwell, K.A., et al. (2013). Yeast reveal a "druggable" Rsp5/Nedd4 network that ameliorates α-synuclein toxicity in neurons. Science *342*, 979–983.

Tofaris, G.K., Kim, H.T., Hourez, R., Jung, J.-W., Kim, K.P., and Goldberg, A.L. (2011). Ubiquitin ligase Nedd4 promotes alpha-synuclein degradation by the endosomal-lysosomal pathway. Proc. Natl. Acad. Sci. U S A *108*, 17004–17009.

Udeshi, N.D., Mani, D.R., Eisenhaure, T., Mertins, P., Jaffe, J.D., Clauser, K.R., Hacohen, N., and Carr, S.A. (2012). Methods for quantification of in vivo changes in protein ubiquitination following proteasome and deubiquitinase inhibition. Mol. Cell. Proteomics *11*, 148–159.

Wagner, S.A., Beli, P., Weinert, B.T., Nielsen, M.L., Cox, J., Mann, M., and Choudhary, C. (2011). A proteome-wide, quantitative survey of in vivo ubiquitylation sites reveals widespread regulatory roles. Mol. Cell. Proteomics *10*, M111.M013284.

Wang, H., Rempel, D.L., Giblin, D., Frieden, C., and Gross, M.L. (2017). Peptide-level interactions between proteins and small-molecule drug candidates by two hydrogen−deuterium exchange MS-based methods: the example of apolipoprotein E3. Anal. Chem. *89*, 10687–10695.

Wang, J., Peng, Q., Lin, Q., Childress, C., Carey, D., and Yang, W. (2010). Calcium activates Nedd4 E3 ubiquitin ligases by releasing the C2 domain-mediated auto-inhibition. J. Biol. Chem. *285*, 12279–12288.

Wild, P., McEwan, D.G., and Dikic, I. (2014). The LC3 interactome at a glance. J. Cell Sci. *127*, 3–9.

Witte, K., Schuh, A.L., Hegermann, J., Sarkeshik, A., Mayers, J.R., Schwarze, K., Yates, J.R., Eimer, S., and Audhya, A. (2011). TFG-1 function in protein secretion and oncogenesis. Nat. Cell Biol. *13*, 550–558.

Yang, B., and Kumar, S. (2010). Nedd4 and Nedd4-2: closely related ubiquitin-protein ligases with distinct physiological functions. Cell Death Differ. *17*, 68–77.

Zambon, F., Cherubini, M., Fernandes, H.J.R., Lang, C., Ryan, B.J., Volpato, V., Bengoa-Vergniory, N., Vingill, S., Attar, M., Booth, H.D.E., et al. (2019). Cellular α-synuclein pathology is associated with bioenergetic dysfunction in Parkinson's iPSC-derived dopamine neurons. Hum. Mol. Genet. *28*, 2001–2013.

Zanzoni, A., Montecchi-Palazzi, L., Quondam, M., Ausiello, G., Helmer-Citterich, M., and Cesareni, G. (2002). MINT: a Molecular INTeraction database. FEBS Lett. *513*, 135–140.

Zhu, M.M., Rempel, D.L., Du, Z., and Gross, M.L. (2003). Quantification of protein-ligand interactions by mass spectrometry, titration, and H/D exchange: PLIMSTEX. J. Am. Chem. Soc. *125*, 5252–5253.

STAR★METHODS

KEY RESOURCES TABLE

REAGENT or RESOURCE	SOURCE	IDENTIFIER
Antibodies		
Anti-ubiquitin, rabbit polyclonal	Abcam	Cat#Ab7780; RRID: AB_306069
Anti-ubiquitin (K63 linkage), rabbit monoclonal	Abcam	Cat#Ab179434
Anti-ubiquitin (K48 linkage), rabbit monoclonal	Abcam	Cat#Ab140601; RRID: AB_2783797
Anti-myc, mouse monoclonal	Santa Cruz Biotechnology	Cat#Sc-40; RRID: AB_627268
Anti-HA, rat monoclonal	Roche	Cat#11867423001; RRID: AB_390918
Anti-Rab5a, rabbit polyclonal	ThermoFisher Scientific	Cat#PA529022; RRID: AB_2546498
Anti-GLG1, rabbit polyclonal	ThermoFisher Scientific	Cat#PA526838; RRID: AB_2544338
Anti-calreticulin, rabbit polyclonal	ThermoFisher Scientific	Cat#PA3900; RRID: AB_325990
Goat anti-mouse HRP	BioRad	Cat#1721011
Goat anti-rabbit HRP	BioRad	Cat#1706515
Anti-rat AlexaFluor488 conjugate	Invitrogen	Cat#A11006
Anti-rabbit AlexaFluor568 conjugate	Invitrogen	Cat#A11011
Anti-actin	Abcam	Cat#Ab14128; RRID: AB_300931
Bacterial and Virus Strains		
BL21(DE3)	EMD Millipore	Cat#69450-3
BL21(DE3)-CodonPlus-RIL	Agilent Technologies	Cat#230240
NEB5α (for Q5 mutagenesis)	New England Biolabs	Cat#C2987
Chemicals, Peptides, and Recombinant Proteins		
N-(2-chlorobenzyl)-4-fluoro-3-nitrobenzamide	Tardiff et al., 2013; This paper	N/A
N-(2-chlorobenzyl)-1-(2,5-dimethylphenyl)-1H-benzo[d]imidazole-5-carboxamide (NAB2)	Tardiff et al., 2013; This paper	N/A
3-amino-N-(2-chlorobenzyl)-4-(m-tolylamino)benzamide (NAB17)	Tardiff et al., 2013; This paper	N/A
SYPRO orange dye	Invitrogen	
Ubiquitin	Pickart and Raasi, 2005; This paper	N/A
Ubch5a	This paper	N/A
UBE1	R&D Systems	Cat#E-304-050
Nedd4(full-length)	Hatstat and McCafferty, 2020; This paper	N/A
Nedd4(HECT)	This paper	N/A
Ubiquitin (^{15}N,^{13}C-labeled)	R&D Systems	Cat#U-700-100
Deposited Data		
Qualitative and quantitative TUBE-coupled proteomics	This paper; Deposited to MassIVE database	ProteomeXchange ID: PXD019245 Password:NEDD4
Experimental Models: Cell Lines		
SHSY5Y	From Duke Cell Culture Facility, via ATCC	ATCC CRL-2266; RRID: CVCL_0019
Oligonucleotides		
pGEX-Nedd4 TEV insertion mutagenesis FWD primer 5'-CACCACCCA CTCCCCTATACTAGGTATTG-3'	Synthesized by Eton Biosciences; This Paper	N/A

(*Continued on next page*)

Continued

REAGENT or RESOURCE	SOURCE	IDENTIFIER
pGEX-Nedd4 TEV insertion mutagenesis REV primer 5'-ATGATGATGC ATGAATACTGTTTCCTGTG-3'	Synthesized by Eton Biosciences; This Paper	N/A
pGEX-Nedd4 His_6 insertion mutagenesis FWD primer 5'-TTTTCAGGGCG CCCTTATGGCAACTTGC-3'	Synthesized by Eton Biosciences; This Paper	N/A
pGEX-Nedd4 His_6 insertion mutagenesis REV primer 5'-TACAGGTTTTCGA ATTCGGGGATCCCACG-3'	Synthesized by Eton Biosciences; This Paper	N/A
Recombinant DNA		
pET15-UbE2D1 (Ubch5a)	Jin et al., 2007	Addgene#15782
pGEX-Nedd4	Hatstat and McCafferty, 2020	
pET15-ubiquitinWT	Brzovic et al., 2006	Addgene#12647
pET28-MHL-5c7J (Nedd4(HECT))	Depositor: Cheryl Arrowsmith; unpublished	Addgene#69965
pCI-HA-Nedd4	Gao et al., 2009	Addgene#27002
pHM6-α-Synuclein-WT	Furlong et al., 2000	Addgene#40824
pHM6-α-Synuclein-A53T	Furlong et al., 2000	Addgene#40825
pCMV-myc-DDK-TFG	OriGene	Cat#RC200293
Software and Algorithms		
PANTHER	Mi et al., 2005; Mi and Thomas, 2009	http://www.pantherdb.org/; RRID: SCR_004869
GOrilla	Eden et al., 2009	http://cbl-gorilla.cs.technion.ac.il/; RID: SCR_006848
BioGrid	Stark et al., 2006	https://thebiogrid.org/; RRID: SCR_007393
IntAct	Hermjakob et al., 2004	https://www.ebi.ac.uk/intact/; RRID: SCR_006944
Mentha	Calderone et al., 3013	https://mentha.uniroma2.it/; RRID: SCR_016148
IMEx	Orchard et al., 2012	https://www.imexconsortium.org/; RRID: SCR_002805
ProteomeDiscoverer	ThermoFisher Scientific	https://www.thermofisher.com/order/catalog/product/OPTON-30810#/OPTON-30810; RRID: SCR_014477
Prism 8	GraphPad	https://www.graphpad.com/scientific-software/prism/; RRID: SCR_002798
Other		
Q5 site-directed mutagenesis kit	New England Biolabs	Cat#E0554
DMEM-F12 media	Gibco via ThermoFisher	Cat#11330032
FBS	Sigma Aldrich	Cat#F-2442
Penicillin-streptomycin	Gibco via ThermoFisher	Cat#15140122
GeneX Plus Transfection Reagent	ATCC	ATCC ACS-4004
Series S CM5 Chip for Biacore SPR analysis	Cytiva (formerly GE Healthcare Life Sciences)	Cat#BR100012
TUBE 1 resin (magnetic bead conjugated)	LifeSensors	Cat#UM401M
Magnetic bead control resin	LifeSensors	Cat#UM400M

RESOURCE AVAILABILITY

Lead Contact

Further information and requests for resources and reagents should be directed and will be fulfilled by the Lead Contact, Prof. Dewey G. McCafferty (dewey.mccafferty@duke.edu).

Materials Availability

Plasmids used in this study were obtained from Addgene plasmid repository or from OriGene and were used as received unless otherwise stated. All plasmids, including Addgene and OriGene accession information, are described in Table S2 and Key Resources Table. Plasmids modified after receipt will be shared upon request by contacting the Lead Contact.

Mammalian cell lines were accessed from the Duke University Cell Culture Facility, which provides access for Duke Users to cell lines sourced via ATCC. ATCC source information is provided in the Key Resources Table.

Synthesis of small molecules is described herein according to previously reported methods. Compounds can be generated according to the described procedure or will be shared upon request by contacting the Lead Contact.

Data and Code Availability

For the proteomics experiments described herein, the raw mass spectrometry proteomics data, the spectral library, Spectronaut.SNE file and associated results and metadata have been deposited in MassIVE (ftp://MSV000085432@massive.ucsd.edu with username MSV000085432 and password "NEDD4") with the ProteomeXchange ID PXD019245.

All other raw data, including HDX-MS and microscopy data, is available upon request.

EXPERIMENTAL MODEL AND SUBJECT DETAILS

SH-SY5Y Mammalian Cell Line

Mammalian SH-SY5Y cells were obtained from the Duke University Cell Culture Facility (via ATCC, Source # CRL-2266) and were maintained at 37°C with 5% CO_2 in DMEM:F12 (1:1; Gibco) supplemented with 10% FBS (Sigma Aldrich) and 1X penicillin-streptomycin (Gibco). This cell line is neuroblastoma derived, immortalized from bone marrow taken from a female (4yo). SH-SY5Y cells were passaged with the recommended sub-cultivation ratio of 1:20 to 1:50 and were used as wild-type cells or transfected as described herein.

Competent E. coli for Protein Production

For recombinant protein production, *E. coli* strains BL21(DE3) (EMD Millipore) and BL21(DE3)-CodonPlus-RIL (Agilent) were used. Strains were propagated and chemically competent cells were generated in the McCafferty lab. For protein production, strains were transformed with the plasmid of interest and cultured in LB media under antibiotic selection (plasmid-specific for BL21(DE3); plasmid-specific and chloramphenicol double selection for BL21(DE3)-CodonPlus-RIL). Specific growth conditions were optimized for each recombinant protein (details presented in Method Details).

METHOD DETAILS

Plasmids

All plasmids used in the described experiments were ordered from Addgene plasmid repository (Table S1). Plasmids were sequenced upon arrival and used as received unless specifically noted. Any modifications to plasmid sequences were generated by Q5 site-directed mutagenesis (New England BioLabs) and confirmed by sequencing. All plasmid information, including accession numbers, expression constructs, and modifications by site-directed mutagenesis, are described in Table S1.

Protein Expression and Purification

All proteins described herein for *in vitro* analyses were expressed and purified as recombinant proteins with the exception of E1 activating enzyme UBE1 and heavy isotope labeled ubiquitin (both purchased from R&D Systems). Recombinant ubiquitin, Ubch5a, Nedd4(HECT), and full-length Nedd4 were accessed by expression in *E. coli* using the expression constructs described in Table S1. For all recombinant proteins described herein, expression and purification details are described below.

General Method

The expression plasmid was transformed into the desired competent *E. coli* strain and were plated on an antibiotic selection plate for overnight growth at 37°C. Starter cultures were inoculated from the selection plate and grown overnight (200 rpm, 37°C). Expression cultures were inoculated from saturated starter culture and OD_{600} was monitored until the desired density at which point expression was induced by addition of isopropyl β-D-1-thiogalactopyranoside (IPTG; GoldBio). Following expression, cells were harvested by centrifugation (Sorvall SLA-3000, 5,000 rpm, 20 min, 4°C, resuspended in lysis buffer, and lysed using an EmulsiFlex C5 homogenizer (Avestin). Cell debris was removed from lysates by ultracentrifugation (Beckman Coulter 70-Ti rotor, 40,000 rpm, 4°C, 0.02 Torr, 45 minutes) and lysates were purified by affinity chromatography via AKTA FPLC (GE Life Sciences).

Ubch5a

pET15-Ubch5a was transformed into BL21(DE3) competent *E. coli* and successful transformants were selected for by growth on an ampicillin selection plate. For expression, a starter culture (100 mL LB media) was inoculated from a streak of colonies on the selection plate and allowed to reach saturation by overnight growth at 37°C. Expression cultures were inoculated from saturated starter culture (10 mL starter culture per 1 L LB media) and grown at 37°C until OD_{600} = 0.6 at which time expression was inducted with the addition of IPTG to a final concentration of 100 μM and grown overnight at 18°C. After growth, cells were harvested and pelleted for storage at −20°C until use for purification. For purification, the cell pellet was thawed on ice and subsequent resuspended in lysis buffer (50 mM Tris, 500 mM NaCl, pH 7.5 with 1X protease inhibitor cocktail, 40 μM PMSF and lysozyme). The cells were lysed and the cell debris was removed from the lysate by ultracentrifugation. Ubch5a was purified from the supernatant of the lysate as follows: the supernatant was loaded onto a Ni^{2+}-charged immobilized metal affinity column (equilibrated with 50 mM Tris, 500 mM NaCl, 20 mM imidazole, pH 7.5). Ubch5a was eluted via gradient elution from 20 to 500 mM imidazole. Ubch5a-containing fractions were pooled dialyzed overnight against 4 L of dialysis buffer (50 mM Tris, 500mM NaCl, pH 7.5) to remove imidazole from the sample. The protein was subsequently concentrated and aliquoted for storage at 4°C, −20°C (in 40% glycerol), and −80°C.

Nedd4(HECT)

pET28-MHL-5C7J was transformed into BL21(DE3) competent *E. coli* and successful transformants were selected for by growth on a kanamycin selection plate. For expression, a starter culture (100 mL LB media) was inoculated from a streak of colonies on the selection plate and allowed to reach saturation by overnight growth at 37°C. Expression cultures were inoculated from saturated starter culture (10 mL starter culture per 1 L LB media) and grown at 37°C until OD_{600} = 0.6 at which time expression was inducted with the addition of IPTG to a final concentration of 500 μM and grown overnight at 18°C. After growth, cells were harvested and pelleted for storage at −20°C until use for purification. For purification, the cell pellet was thawed on ice and subsequently resuspended in lysis buffer (50 mM Tris, 500 mM NaCl, pH 7.5 with 1X protease inhibitor cocktail, 40 μM PMSF and lysozyme). The cells were lysed and the cell debris was removed from the lysate by ultracentrifugation. Nedd4(HECT) was purified from the supernatant of the lysate as follows: the supernatant was loaded onto a Ni^{2+}-charged immobilized metal affinity column (equilibrated with 50 mM Tris, 100 mM NaCl, 20 mM imidazole, pH 7.5). Nedd4(HECT) was eluted via gradient elution from 20 to 250 mM imidazole. Nedd4(HECT)-containing fractions were pooled dialyzed overnight against 4 L of dialysis buffer (50 mM Tris, 100mM NaCl, pH 7.5, 1 mM TCEP), and His_6-TEV protease (1 mg) was added into the dialysis tubing with Nedd4(HECT) for proteolytic cleavage of the hexahistidine tag. After overnight dialysis, Nedd4(HECT) was subsequently purified through an additional round of Ni^{2+}-charged immobilized metal affinity (with buffers as stated above), and untagged Nedd4(HECT) was collected in the flow-through or from the wash while His_6-TEV protease was separated from the desired protein. Nedd4(HECT) was subsequently concentrated and aliquoted for storage at 4°C, −20°C (in 40% glycerol), and −80°C.

Nedd4 (Full-Length)

Nedd4 was purified according to our previously optimized method (Hatstat and McCafferty, 2020). pGEX-Nedd4 (after two rounds of site-directed mutagenesis for insertion of hexahistidine affinity tag and TEV protease cleavage sequence) was transformed into BL21(DE3)-CodonPlus-RIL competent *E. coli*. Successful transformants were selected for by growth on ampicillin/chloramphenicol double selection plates. For expression, a starter culture (100 mL LB media) was inoculated from a streak of colonies on the selection plate and allowed to reach saturation by overnight growth at 37°C. Expression cultures were inoculated from saturated starter culture (10 mL starter culture per 1 L LB media) and grown at 37°C until OD_{600} = 0.6 at which time expression was inducted with the addition of IPTG to a final concentration of 100 μM and grown overnight at 18°C. After growth, cells were harvested and used immediately for purification. The cell pellet was resuspended in lysis buffer (50 mM Tris, 250 mM NaCl, pH 7.4 with 1X protease inhibitor cocktail, 40 μM PMSF and lysozyme). The cells were lysed and the cell debris was removed from the lysate by ultracentrifugation. His_6-GST-Nedd4 was purified from the supernatant of the lysate as follows: the supernatant was loaded onto glutathione agarose column (Genesee Scientific) that had been pre-equilibrated with 50 mM Tris, 250 mM NaCl, pH 7.4. The column was washed with 10 column volumes of buffer and His_6-GST-Nedd4 was eluted with 7 column volumes of elution buffer (50 mM Tris, 250 mM NaCl, pH 7.4 with 20 mM glutathione reduced). His_6-GST-Nedd4 containing fractions were pooled dialyzed overnight against 4 L of dialysis buffer (50 mM Tris, 100mM NaCl, pH 7.5, 1 mM β-mercaptoethanol), and His_6-TEV protease (1 mg) was added into the dialysis tubing with Nedd4 for proteolytic cleavage of the His_6-GST tag. After overnight dialysis, Nedd4 was subsequently purified through Ni^{2+}-charged immobilized metal affinity chromatography wherein the resin was pre-equilibrated with wash buffer (50 mM Tris, 250 mM NaCl, pH 7.4 with 20 mM imidazole). Dialysate was loaded onto the equilibrated column and untagged Nedd4 was collected in the flow-through and early in a 10 column volume wash. His_6-TEV and cleaved His_6-GST were eluted from the column over a gradient elution from 20 to 250 mM imidazole. Untagged full-length Nedd4 was subsequently concentrated and aliquoted for storage at 4°C, −20°C (in 40% glycerol).

Ubiquitin

Ubiquitin purification was based on a method previously described (Pickart and Raasi, 2005). pET15-ubiquitin was transformed into BL21(DE3) competent *E. coli* and successful transformants were selected for by growth on ampicillin selection plates. For expression, a starter culture (100 mL 2xYT media) was inoculated from a streak of colonies on the selection plate and were grown at 37°C until OD_{600} = 0.6. Expression cultures were inoculated from starter culture (10 mL starter culture per 1 L 2xYT media) and grown at 37°C until OD_{600} = 0.6 at which time expression was inducted with the addition of IPTG to a final concentration of 400 μM and for four additional hours at 37°C. After growth, cells were harvested and pellets were stored at −20°C until use for purification. For purification, cell pellets were thawed on ice and resuspended in lysis buffer (50 mM Tris pH 7.6, 1 mM phenylmethylsulfonyl fluoride,

1X protease inhibitor cocktail (Bimake) and 0.4 mg/mL lysozyme). Cells were subsequently lysed and cell debris was removed by centrifugation (Sorvall SS-34, 8000 rpm, 20 min at 4°C). Supernatant was transferred to a cooled beaker on ice and perchloric acid (70%, 0.35 mL per 50 mL lysis buffer used) was added while stirring. Solution was centrifuged (Sorvall SS-34, 8000 rpm, 20 min at 4°C) and supernatant was dialyzed against 2L dialysis buffer (50 mM ammonium acetate, pH 4.5) overnight. Dialysis tubing was transferred to 2L fresh dialysis buffer and dialyzed for an additional few hours. After dialysis, ubiquitin was further purified by ion exchange chromatography using SP Sepharose (column equilibrated with 50 mM ammonium acetate, pH 4.5) and was eluted over a gradient elution from 0 to 0.5 M NaCl in 50 mM ammonium acetate. Fractions were analyzed by SDS-PAGE and fractions containing ubiquitin were pooled and concentrated. Samples were lyophilized or buffer exchanged into desired assay reaction buffers.

Site-Directed Mutagenesis

All site-directed mutagenesis was performed following Q5 site-directed mutagenesis kit and published manufacturer's protocol (New England Biolabs). Two rounds of mutagenesis were performed for insertion of a hexahisitidne sequence and a cleavage sequence for TEV protease into the pGEX-Nedd4 plasmid. Primers used for mutagenesis were designed with NEBaseChanger (New England Biolabs) and are described in Table S2. Mutagenesis was confirmed by Sanger sequencing as performed by Eton Biosciences.

Small Molecule Synthesis

Materials

Unless otherwise stated, all reagents were purchased from either Sigma-Aldrich or Oakwood Chemicals and were used as received. $CDCl_3$ was purchased from Cambridge Isotope Laboratories and used as received.

Characterization

NMR spectra were obtained using Bruker Advance Neo - 500 MHz multinuclear spectrometer (Duke Chemistry NMR Facility) operating at 500, MHz for ^{1}H NMR and 126 MHz for ^{13}C NMR and are reported as chemical shifts (δ) in parts per million (ppm). Spectra were referenced internally according to residual solvent signals (^{1}H, $CDCl_3$ 7.26 ppm; ^{13}C, $CDCl_3$ 77.0 ppm). Data for NMR spectra use the following abbreviations to describe multiplicity: s, singlet; br s, broad singlet; d, doublet; t, triplet; dd, doublet of doublets; td, triplet of doublets; tt, triplet of triplets; ddd, doublet of doublets of doublets; dddd, doublet of doublets of doublets of doublets; ddt, doublet of doublets of triplets; app dd, apparent doublet of doublets; m, multiplet. Coupling constants (J) are reported in units of hertz (Hz). High-resolution mass spectra (HRMS, m/z) were recorded on an Agilent 6224 LC/MS-TOF spectrometer using electrospray ionization (ESI, Duke University Department of Chemistry Shared Instrumentation Facility).

Preparation of N-arylbenzimidaozle (NAB) derivatives

N-arylbenzimidazole derivatives NAB2 and NAB17 were synthesized according to previously reported procedures (Tardiff et al., 2013) as described below. Characterization via NMR and HRMS are consistent with previously reported characterizations.

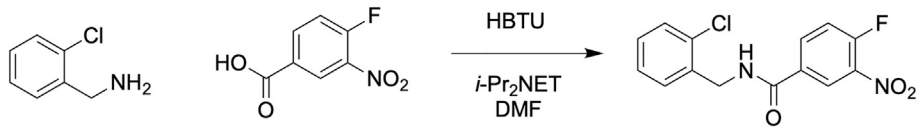

N-(2-chlorobenzyl)-4-fluoro-3-nitrobenzamide. 2-Chlorobenzylamine (0.71 mL, 6.0 mmol) was added slowly to a stirred solution of 4-fluoro-3-nitrobenzoic acid (925 mg, 5.0 mmol), HBTU (1.90 g, 5.0 mmol), *N*,*N*-diisopropylethylamine (1.05 mL, 6.0 mmol), and DMF (10 mL) at room temperature. After 30 min, the solution was diluted with ethyl acetate (50 mL) and washed sequentially with water, 1M HCl (aq) (3X), 1M KOH (aq) (3X), and brine. The organic layer was dried over sodium sulfate, filtered, and concentrated under reduced pressure using a rotary evaporator. Purification of the residue by silica gel chromatography (10-45% EtOAC/Hexanes; material loaded using toluene) provided the title compound as a yellow solid (0.77 g, 50% yield). ^{1}H NMR (500 MHz, $CDCl_3$) δ 8.46 (dd, J = 7.0, 2.3 Hz, 1H), 8.11 (ddd, J = 8.8, 4.1, 2.3 Hz, 1H), 7.50 – 7.34 (m, 4H), 7.28 (m, 2H), 6.60 (s, 1H), 4.75 (d, J = 5.9 Hz, 2H). ^{13}C NMR (126 MHz, $CDCl_3$) δ 164.30, 157.24 (d, J = 270.9), 134.96, 134.67 (d, J = 8.8), 133.73, 131.18 (d, J = 3.8) 130.28, 129.72, 129.33, 127.25, 125.2, 118.95 (d, J = 21.4), 42.43. HRMS (ESI-TOF) *m/z* calcd for $C_{14}H_{10}ClFN_2O_3$ $[M+H]^+$ 309.0437, found 309.0445.

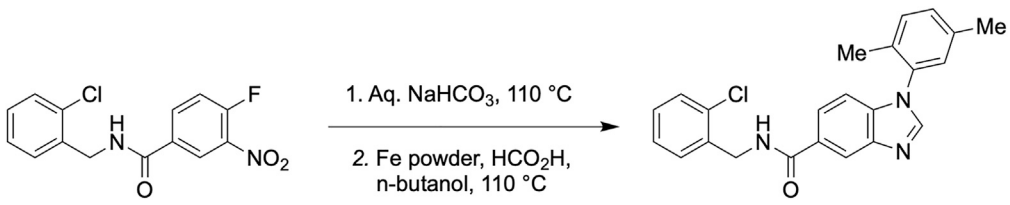

N-(2-chlorobenzyl)-1-(2,5-dimethylphenyl)-1H-benzo[d]imidazole-5-carboxamide (NAB2). A screw-top test tube containing N-(2-chlorobenzyl)-4-fluoro-3-nitrobenzamide (0.96 mmol, 300 mg), sodium bicarbonate (1.92 mmol, 161 mg), 2,5-dimethylaniline (1.92 mmol, 240 μL), and water (2 mL/mmol benzamide) was sealed with a Teflon screw cap, placed in a preheated oil bath at

110°C, and stirred for 24 h. The reaction was cooled to room temperature and the mixture was poured onto ethyl acetate (sufficient volume for all solid to be dissolved). The solution washed sequentially with 1M HCl (aq) (3X), water (3X), and brine (3X). The organic layer was dried over sodium sulfate, filtered, and concentrated using reduced pressure via a rotary evaporator. The crude nitroaniline was subsequently dissolved in n-butanol (1.0 mL/mmol benzamide, 0.96 mL), transferred to a second screw-top test tube, and formic acid (1.0 mL/mmol benzamide, 0.96 mL), iron powder (9.6 mmol, 536 mg), and concentrated HCl (0.1 mL/mmol benzamide, 96 μL) were added to the solution. The test tube was sealed with a Teflon screw cap and stirred for 1 h at 110°C. After cooling to room temperature, the mixture was poured onto a mixture of ethyl acetate and saturated $NaHCO_3$ (1:6 ratio) in a separatory funnel. The mixture was shaken with venting and solid sodium bicarbonate added until pH∼12. The layers were separated, and the organic layer was washed with water (3X), dried and concentrated under reduced pressure. The residue was purified by silica gel chromatography using 40-100% EtOAC/Hexanes (material loaded using chloroform) to afford NAB2 as a white solid (194.1mg, 52% yield). ^{1}H NMR (500 MHz, $CDCl_3$) δ 8.27 (s, 1H), 8.01 (s, 1H), 7.83 (dd, J = 8.5, 1.7 Hz, 1H), 7.52 (dd, J = 7.0, 2.4 Hz, 1H), 7.40 (dd, J = 7.0, 2.2 Hz, 1H), 7.31 (d, J = 7.9 Hz, 1H), 7.29 – 7.22 (m, 3H), 7.18 (d, J = 8.5 Hz, 1H), 7.11 (s, 1H), 6.71 (bs, 1H), 4.79 (d, J = 5.9 Hz, 2H), 2.40 (s, 3H), 2.03 (s, 3H). ^{13}C NMR (126 MHz, $CDCl_3$) δ 167.85, 144.65, 143.01, 137.45, 137.01, 136.00, 134.14, 133.78, 132.04, 131.53, 130.55, 130.37, 129.67, 129.27, 129.03, 128.10, 127.27, 123.49, 119.26, 110.91, 42.24, 20.89, 17.19. HRMS (ESI-TOF) *m/z* calcd for $C_{23}H_{20}ClN_3O$ $[M+H]^+$ 390.1368, found 390.1371.

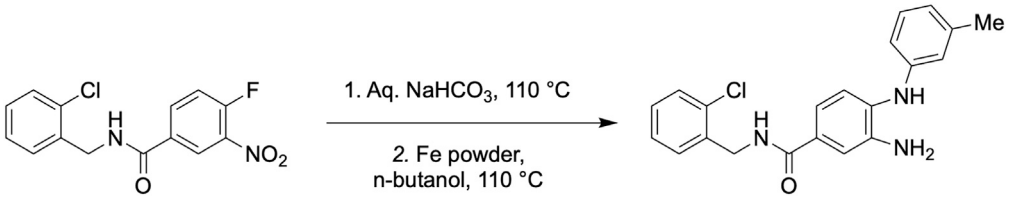

3-amino-N-(2-chlorobenzyl)-4-(m-tolylamino)benzamide (NAB17). A screw-top test tube containing N-(2- chlorobenzyl)-4-fluoro-3-nitrobenzamide (0.32 mmol, 100 mg), sodium bicarbonate (0.64 mmol, 53 mg), 3-methylaniline (0.64 mmol, 68 μL), and water (2 mL/mmol benzamide) was sealed with a Teflon screw cap, placed in a preheated oil bath at 110°C, and stirred for 24 h. The reaction was cooled to room temperature and the mixture was poured onto ethyl acetate (sufficient volume for all solid to be dissolved). The solution washed sequentially with 1M HCl (aq) (3X), water (3X), and brine (3X). The organic layer was dried over sodium sulfate, filtered, and concentrated using reduced pressure via a rotary evaporator. The crude nitroaniline was subsequently dissolved in n-butanol (1.0 mL/mmol benzamide, 0.32 mL), transferred to a second screw-top test tube, iron powder (3.2 mmol, 179 mg), and concentrated HCl (0.1 mL/mmol benzamide, 0.032 mL) were added to the solution. *NOTE*: *formic acid was omitted from this reaction mixture to prevent closure of the heterocycle*. The test tube was sealed with a Teflon screw cap and stirred for 1 h at 110°C. After cooling to room temperature, the mixture was poured onto a mixture of ethyl acetate and saturated $NaHCO_3$ (1:6 ratio) in a separatory funnel. The mixture was shaken with venting and solid sodium bicarbonate added until pH∼12. The layers were separated, and the organic layer was washed with water (3X), dried and concentrated under reduced pressure. The crude product was worked up as described and purified by silica gel chromatography using 40-100% EtOAC/Hexanes (material loaded using chloroform) to afford NAB17 as an off-white solid (72.7 mg, 62.1%). ^{1}H NMR (500 MHz, $CDCl_3$) δ 7.50 – 7.44 (m, 1H), 7.39 (dd, *J* = 7.2, 2.2 Hz, 1H), 7.31 (d, *J* = 2.0 Hz, 1H), 7.25 – 7.20 (m, 2H), 7.17 – 7.08 (m, 3H), 6.74 (d, *J* = 7.6 Hz, 1H), 6.69 (d, *J* = 6.2 Hz, 2H), 6.49 (m, 1H), 5.33 (s, 1H), 4.72 (d, *J* = 6.0 Hz, 2H), 2.29 (s, 3H), 2.01 (d, *J* = 1.2 Hz, 1H). ^{13}C NMR (126 MHz, $CDCl_3$) δ : 167.30, 143.44, 139.53, 139.46, 135.97, 133.86, 133.81, 130.58, 129.70, 129.56, 129.42, 129.12, 127.32, 121.90, 120.57, 118.06, 117.93, 115.86, 114.44, 42.13, 21.66. HRMS (ESI-TOF) *m/z* calcd for $C_{21}H_{20}ClN_3O$ $[M+H]^+$ 366.1368, found 366.1376.

Mammalian Tissue Culture

SHSY5Y cells were obtained from the Duke University Cell Culture Facility and were maintained at 37°C with 5% CO_2 in DMEM:F12 (1:1; Gibco) supplemented with 10% FBS (Sigma Aldrich) and 1X penicillin-streptomycin (Gibco). Cells were passaged at 80% confluency with a sub-cultivation ratio of 1:20 unless seeding for transfection experiments where a higher density was required. Transfection of SHSY5Y was performed with GeneX Plus (ATCC). Transfected plasmids are described in Table S1.

Surface Plasmon Resonance for Low Molecular Weight Kinetics

NAB2 binding to GST-Nedd4 and Nedd4(HECT) was characterized via SPR using the Biacore T200 instrument (GE Life Sciences). Recombinant protein was purified as described with an additional purification step using size exclusion chromatography to ensure high purity prior to use in SPR. SPR analyses were performed with sterile filtered, degassed PBS. Protein was immobilized to a Series S CM5 chip using NHS crosslinking to a surface RU of 7,000-9,000 to provide high density for low molecular weight kinetics. Following immobilization and equilibration, the protein surface was exposed to a concentration gradient of NAB2 (0 to 100 μM in PBS with <1% DMSO for solubility). Binding was calculated with 1:1 binding algorithm for low molecular weight kinetics.

Protein Thermal Shift Assay for Measurement of Ligand-Induced Protein Stability Changes

Nedd4(HECT) or full-length Nedd4 (4 μM) was incubated with NAB2 at various concentrations for 30-60 minutes. Following incubation, SYPRO orange (5000X stock in DMSO, Invitrogen) was added to a final concentration of 5X and mixtures were aliquoted to a final volume of 15 μL into a LightCycle 96-well white qPCR plate (Roche). Thermal denaturation was conducted in a LightCycler 480 (Roche) via continuous heating from 20 to 85°C over 18 minutes. Experimental T_m was calculated as the absolute minimum of the negative first derivative curve of the melting curve (-d(fluorescence intensity)/d(temperature)).

Ubiquitination Activity Assay by Immunoblotting

In vitro ubiquitination activity assays were conducted as endpoint assays via immunoblot detection using recombinant E1, E2, and E3 enzymes. E1 (100 nM), E2 (1 μM) and E3 (5 μM) were incubated with ubiquitin (100 μM) in reaction buffer (100 mM Tris, 25 mM $MgCl_2$, 0.1% Tween, pH 8) and reaction was initiated by addition of ATP (2 mM). Reactions were incubated for 1 hour at 37°C and quenched with the addition of SDS-PAGE loading buffer. Samples were heated to 95°C for 10 minutes and separated by SDS-PAGE. Gels were transferred to PVDF membrane for immunoblotting and ubiquitination activity was detected by blotting with anti-ubiquitin (1:2000, Abcam ab7780) or linkage specific antibodies (Abcam: anti-ub(K63), ab179434; anti-ub(K48), ab140601) and HRP-conjugated secondary antibody (BioRad). Signal was detected with ECL reagents (Genesee Scientific) and quantified using ImageJ.

For *in vitro* analysis of TFG ubiquitination, the general method as described above was followed with the exception that 20 μg of SHSY5Y lysate containing overexpressed myc-DDK-TFG (Origene plasmid # RC201093) was added as substrate. TFG ubiquitination was detected with anti-myc primary antibody (1:1000 Santa Cruz Biotechnology, sc-40) and HRP-conjugated anti-mouse secondary antibody (1:1000, BioRad).

MALDI-TOF Ubiquitin Activity Assay

Ubiquitination activity was quantified in a time-dependent manner by MALDI-TOF detection of monoubiquitin consumption according to a procedure adapted from De Cesare et al. (De Cesare et al., 2018). E1 (50 nM), E2 (250 nM), and E3 (500 nM) were combined in reaction buffer composed of 0.25 mg/mL BSA in 10 mM HEPES pH 8.5, 10 mM $MgCl_2$ and 1 mM ATP. Reactions were incubated at 37°C and initiated with the addition of ubiquitin (10 μM). At desired time intervals, an aliquot (5 μL) was quenched with 10% TFA (1 μL). Following collection of all time points, samples were doped with DHAP matrix and 4 μM ^{15}N,^{13}C-ubiquitin as an internal standard (3:1:2 matrix:standard:sample) and spotted on an AnchorChip 384 BC plate (Bruker Daltonics). Samples were analyzed by MALDI-TOF (Bruker Autoflex Speed LRF MALDI-TOF System) using the following automated AutoXecute method: Reflector Positive mode with laser intensity at 80%, Laser Fuzzy Control switched off, and accumulation parameters set to 4000 satisfactory shots in 500 shot steps with movement parameters set to "Walk on Spot". Spectra were accumulated by FlexControl software and processed using FlexAnalysis software. Monoubiquitin signal was normalized to signal from the heavy isotope derivative and plotted as normalized intensity versus time to determine time-dependent ubiquitination activity of the signaling cascade.

Hydrogen-Deuterium Exchange Mass Spectrometry (HDX-MS)

Full-length recombinant Nedd4 (50 μM) was pre-incubated with NAB2 or DMSO control and then exposed to deuterated buffer to HDX analysis at time points ranging from 10 sec to 3 hr. Following exchange, the reaction was quenched to pH 2.4 with cooled quenching buffer (4°C) to prevent back exchange of deuterium, and the sample was submitted to sequential pepsin digestion and desalting via a C18 column (at 4°C) in line with liquid chromatography coupled tandem mass spectrometry (LC-MS/MS) for peptide identification. Peptide coverage and identity were determined using SEQUEST software with the Nedd4 sequence as reference. Relative deuterium uptake of each peptide was determined by comparison to the non-deuterated ("all hydrogen") control using the ExMS2 program, (Kan et al., 2019) and NAB2-dependent changes in the rate of deuterium uptake were determined by comparison of the NAB2-treated sample relative to the DMSO control. Heat maps were replotted using open source Morpheus program (Broad Institute) and relative deuterium uptake was compared between NAB2-treated and DMSO control.

Qualitative Proteomic Analysis of TUBE-enriched Ubiquitylome

SHSY5Y cells were seeded in 150 mm tissue culture plates and grown in DMEM/F12 (1:1) supplemented with 10% FBS and penicillin/streptomycin (1X). When cells were 80% confluent, a treatment time course was initiated. Cells were treated for 6, 12, 18, and 24 hours with 20 μM NAB2 in DMSO (and a DMSO control at 24 hour timepoint). Following treatment, cells were harvested and resuspended in TUBE lysis buffer (50mM Tris-HCl, pH 7.5, 0.15M NaCl, 1mM EDTA, 1% NP-40, 10% glycerol, published by LifeSensors, Inc.) with 1X protease inhibitor cocktail (Bimake) and 50 μM PR-619 (non-specific DUB inhibitor, Sigma). Cells were then sonicated (Fisher Scientific Model 120 Sonic Dismembrator; 4 pulses, 5 seconds per pulse, 30% amplitude) and cell debris was collected by centrifugation (14,000 rpm, 4°C, 10 minutes). Lysate concentration was determined by Bradford assay. Magnetic TUBE 1 beads (pan-selective) were equilibrated by washing with TBS-T and lysate was added to TUBE beads to a final ratio of 100 μL bead slurry to 1 mg total protein. An additional sample was prepared with magnetic control beads (LifeSensors) and DMSO-treated lysate. Lysate was incubated with TUBE beads or control beads for 2 hours at 4°C with end-over-end rotation. Following incubation, beads were collected and supernatant was removed. Beads were washed with TBST and bound protein was eluted for proteomic analysis with 50 mM TEAB buffer containing 5% SDS. Subsequently, a BCA assay was performed on the samples. The control pulldown had ~0.3 μg/μl and the other samples were 0.55, 0.52, 0.59, 0.5 and 0.53 μg/μl (for DMSO-treated, 6hr, 12hr, 18hr, and 24 hr timepoints, respectively). 25 μL of each sample was reduced and alkylated, followed by clean up and digestion with trypsin using an S-Trap

(Protifi). After lyophilization, tryptic digests were resuspended in 12 μL, and 1 μL of each sample was analyzed by LC-MS/MS (see below) followed by database searching using Mascot. Search results were annotated at a 1% peptide/protein FDR in Scaffold.

Quantitative Proteomic Analyses of TUBE-Enriched Ubiquitylome

Fifty microliters of eluents were diluted to 75 μL with 10% SDS in 50 mM triethylammonium bicarbonate (TEAB) buffer. Samples were reduced by heating with 10 mM DTT at 80 °C for 10 min. Next, reduced thiols were alkylated with 25 mM iodoacetamide at room temperature for 30 min. Finally, samples were processed using an S-Trap micro device (Protifi) using the manufacturer's protocol. Digestion of each sample was performed using 1 μg of Sequencing Grade Modified Trypsin (Promega) in TEAB per sample at 47 °C for 1 h. After elution from the S-Trap, peptides were lyophilized and resuspended in 12 μl of 1% TFA/ 2% MeCN. A QC pool was made by combining an equi-volume of each sample.

Quantitative one-dimensional liquid chromatography, tandem mass spectrometry (1D-LC-MS/MS) was performed on 4.5 μL of the peptide digests per sample in singlicate based on an initial loading study. After two conditioning runs with the QC pool, samples were analyzed in a batch-randomized manner with interspersed QC pools. The LC-MS/MS used a nanoACQUITY UPLC system (Waters) coupled to a Thermo Fusion Lumos high resolution accurate mass tandem mass spectrometer (Thermo) via a nanoelectrospray ionization source and FAIMS Pro Interface. Briefly the sample was first trapped on a Symmetry C18 180 μm × 20 mm trapping column (5 μl/min at 99.9/0.1 v/v H2O/MeCN) followed by an analytical separation using a 1.7 μm ACQUITY HSS T3 C18 75 μm × 250 mm column (Waters) with a 90 min gradient of 5 to 30% MeCN with 0.1% formic acid at a flow rate of 400 nl/min and column temperature of 55°C. Data collection on the Fusion Lumos MS was performed in data-dependent acquisition (DDA) mode with a 120,000 resolution (@ m/z 200) full MS scan from m/z 375 to 1600, with a compensation voltage (CV) of -40, -60 or -80, and a target AGC value of 2e5 ions and 50 ms maximum injection time (IT) with internal calibration enabled. Peptides were selected for MS/MS using with advanced peak determination enabled, peptide monoisotopic peak determination, and including charge states 2-5. MS/MS used HCD fragmentation and detection in the ion trap. For each CV, a 0.66 s method used an isolation width of 1.2 m/z, a normalized collision energy of 30 ± 5%, a rapid ion trap scan rate, normalized AGC target of 100% and auto IT. A 20 s dynamic exclusion was enabled.

Following the MS analysis, data was processed using Proteome Discoverer 2.4 (Thermo). Data processing used Minora Feature Detector with min. trace length of 3, max. ΔRT of isotope patterns of 0.2 min, and PSM confidence of at least medium. Database searching was performed using Mascot 2.4 using a Swissprot database with homo sapiens taxonomy (downloaded on 031119; 20,358 unique sequences; with bovine casein appended) with trypsin specificity, up to 2 missed cleavages, precursor mass tolerance of 5 ppm, fragment mass tolerance of 0.8 Da, static carbamidomethyl(C), variable oxidation(M), deamidation(NQ) and GG(K). For label-free quantification (LFQ), Minora feature mapper used a trace length of 3 and max ΔRT of 0.2. Default percolator settings were used for FDR determination. Consensus steps used the Feature Mapper with RT alignment and a max RT shift of 5 min and min S/N threshold of 1. The precursor ions quantified used unique+razor peptides and intensity precursor abundance. Normalization was to total peptide Protein abundances were calculated using summed peptide abundances, and imputation used replacement of missing values with random values sampled from the lower five percent of detected values. Data was exported for master proteins that met a high confidence (1% peptide and protein) FDR. Statistical analysis in Proteome Discoverer used ANOVA.

The raw mass spectrometry proteomics data, the spectral library, Spectronaut.SNE file and associated results and metadata have been deposited in MassIVE (ftp://MSV000085432@massive.ucsd.edu with password "NEDD4") with the ProteomeXchange ID PXD019245.

Bioinformatic Analysis of Nedd4 Interactome and Ubiquitylome

Nedd4 interactome information was compiled from various protein-protein interaction databases including BioGrid (Stark et al., 2006), InnateDB (Lynn et al., 2008), MINT (Zanzoni et al., 2002), Mentha (Calderone et al., 2013), IntAct(Hermjakob et al., 2004), and IMEx (Orchard et al., 2012). The compiled interactome was screened for redundancy prior to analyses. The compiled interactome was visualized by Cytoscape and was used for cross-reference to proteins identified from proteomic analyses.

Ubiquitylome proteins identified by proteomic analyses were annotated using the PANTHER functional classification system (Mi et al., 2005). Proteins were annotated for biological process (function) and sub-cellular compartmentalization for organelle localization.

Subcellular Fractionation and Immunoblotting

SHSY5Y cells were seeded into 6-well plates and were transfected with pCI-HA-Nedd4. At 48 hpt, cells were treated with DMSO control or NAB2 (20 μM) in 6 hour intervals. Following treatment, proteins were harvested from the cells by subcellular fractionation using ProteoExtract subcellular fractionation kit (Millipore Sigma). Fractionated samples were analyzed by SDS-PAGE and electrophoresis for detection of HA-tagged Nedd4 (Roche anti-HA high affinity,1:2000 dilution, catalog no. 11867423001) and actin (anti-actin, 1:2000, Abcam ab12148). Nedd4 signal was quantified by ImageJ,(Schindelin et al., 2012) normalized to actin loading control signal, and plotted as percentage of total normalized HA-Nedd4 signal.

Immunofluorescence Microscopy for Protein Translocation Experiments

SHSY5Y cells were seeded for transfection and were subsequently (24h post-seeding) transfected with pCI-HA-Nedd4 or pCDNA3.1 vector control using GeneX Plus Transfection reagent (ATCC). Forty-eight hours post-transfection, cells were treated with NAB2

(20 μM) or DMSO control at 6 hour intervals. Following treatment, cells were fixed using cold methanol and blocked with 3% BSA in TBST for 30 minutes. Following blocking, cells were treated with anti-HA (Pierce High-Affinity, Roche) primary antibody and primary antibody for the trafficking marker of interest (anti-RAB5a, Fisher PA529022; anti-GLG1, Fisher PA526838; anti-calreticulin, Fisher PA3900) for one hour and then with species-specific AlexaFluor conjugated secondary antibodies and Hoechst stain. Cover slips were fixed on microscopy slides and analyzed using a Zeiss AiryScan 880 confocal microscope using the 40X oil objective. Images were processed using Imaris software. Quantitation of co-localization was determined by defining single cells expressing transfected HA-Nedd4 as regions of interest (ROI) and calculating the Pearson's Correlation Coefficient (PCC) across the full volume (z-stack) of the ROI. A minimum of 15 ROI across three separate microscopy frames were measured for each condition and PCC was reported as average ± s.e.m. for comparison of NAB2 treated (3, 6, 12 hr post-treatment) vs time = 0 control.

QUANTIFICATION AND STATISTICAL ANALYSES

For quantitative proteomic analyses, all conditions (experimental and controls) were prepared in triplicate (i.e. n = 3 biological replicates). Following sample enrichment and processing as described above, samples were analyzed by LC-MS/MS wherein two conditioning runs were performed with the QC pool, then samples were analyzed in a batch-randomized manner with interspersed QC pools. Quantitation was performed with label-free quantitative analyses as described above, and statistical analysis was performed on normalized protein abundances via ProteomeDiscoverer using ANOVA analysis. Significant hits were determined using ± 2-fold change and $p < 0.05$ cutoffs. Data was visualized using Prism GraphPad and presented as volcano plots or abundance ratio plots in Figure 5. Raw data and statistical analysis results are available in the MassIVE Proteomics data repository (ftp://MSV000085432@massive.ucsd.edu with password "NEDD4" with the ProteomeXchange ID PXD019245).

For all other experiments with the exception of HDX, samples were prepared in triplicate and quantified data is presented as mean ± s.e.m of three experimental replicates. HDX was performed with a single replicate at each timepoint for each condition. Image quantification was performed with ImageJ for immunoblotting experiments and using Imaris for microscopy experiments. Co-localization in microscopy experiments was calculated with Imaris and statistical differences between experimental and control conditions was determined using a student's t-test. Data visualization and statistical analyses were performed via Prism GraphPad.

Quantification methods and statistical analyses are also described in figure legends and in respective Methods sections.